Global dynamics in a stage-structured discrete-time population model with harvesting

Eduardo Liz[a], Paweł Pilarczyk[b,*]

[a] *Departamento de Matemática Aplicada II, Universidade de Vigo, E.T.S.E. Telecomunicación, Campus Marcosende, 36310 Vigo, Spain*
[b] *Centro de Matemática, Universidade do Minho, Campus de Gualtar, 4710-057 Braga, Portugal*

Abstract

The purpose of this paper is to analyze the effect of constant effort harvesting upon global dynamics of a discrete-time population model with juvenile and adult stages. We consider different scenarios, including adult-only mortality, juvenile-only mortality, and equal mortality of juveniles and adults. In addition to analytical study of equilibria of the system, we analyze global dynamics by means of an automated set-oriented rigorous numerical method. We obtain a comprehensive overview of the dynamics as the harvest rate and survival probability change. In particular, we determine the range of parameters for which the population abundance gets larger in spite of an increase in the harvest rate (so-called *hydra effect*), and for which subsequent increases in harvesting effort can magnify fluctuations in population abundance (destabilize it) and then stabilize it again (so-called *bubble effect*).

Keywords: nonlinear difference equations, age structure, Ricker map, constant effort harvesting, population abundance, hydra effect, bubble effect, equilibrium, stability, periodic orbit, synchronous orbit, oscillations, saddle-node configuration, global dynamics, Morse decomposition, Conley index, attractor, isolating neighborhood, rigorous numerics, set-oriented computations, interval arithmetic
2010 MSC: 37N25, 37B25, 37B35, 39A30, 92-04

1. Introduction

The effects of increasing mortality in various populations are a very important issue from different points of view. In particular, determining these effects

*Corresponding author.
Email addresses: eliz@dma.uvigo.es (Eduardo Liz), pawel.pilarczyk@math.uminho.pt (Paweł Pilarczyk)
URL: http://www.pawelpilarczyk.com/ (Paweł Pilarczyk)

Preprint of a paper published in Journal of Theoretical Biology, Vol. 297 (2012), pp. 148-165.

is vital for optimal management of renewable resources and for control of invasive species. It is commonly accepted that harvesting helps stabilizing the population, and an increase in mortality should typically lead to a decrease in the population stock. However, recent studies indicate that this is not always the case. On the one hand, it turns out that greater mortality can in some cases increase population size [1–5]; on the other hand, it was found out that increasing mortality can magnify fluctuations in population abundance, as was first noticed by Beddington and May [6]. More recent papers exploring this effect are [4, 7–10]; in particular, Abrams and Quince [7] prove that higher predator mortality can be destabilizing in a predator–prey model with a structured prey population when stage length is sufficiently short.

In order to shed some new light on these issues, and to provide a more rigorous analysis on how harvesting influences the dynamics, in this paper we study a simple stage-structured model with two age classes (juveniles and adults), recently introduced in [4]. If A_n and J_n denote the amounts of adults and juveniles after n generations, respectively, then the model equations can be written as follows:

$$\begin{aligned} A_{n+1} &= (1-h_j)s_j J_n + (1-h_a)s_a A_n \\ J_{n+1} &= g((1-h_a)A_n) \end{aligned} \tag{1}$$

where $h_a, h_j \in [0,1]$ are harvest rates of adults and juveniles, respectively; $s_a, s_j \in [0,1]$ are the corresponding survivorship rates, and $g\colon [0,\infty) \to [0,\infty)$ is the stock-recruitment function. We will work with the Ricker map [11]

$$g(x) = \alpha x e^{-\beta x} \tag{2}$$

with $\alpha > 1, \beta > 0$, but similar analysis can be done for other overcompensatory recruitment models. The model assumes that harvest occurs prior to breeding, surviving juveniles become adults after one time step, and adults are capable of surviving several seasons.

As in [4], we will focus on three main harvest strategies, which can be applied in practice and give insight into what happens in the case of other harvest options to kill juveniles and adults with different relative proportions:

$\mathrm{H_a}$: adult-only harvest ($h_j = 0$ and $h_a > 0$)
$\mathrm{H_j}$: juvenile-only harvest ($h_a = 0$ and $h_j > 0$)
$\mathrm{H_e}$: targeting both stages in equal proportion ($h_a = h_j > 0$)

For example, pest control is usually stage-specific, that is, it is frequently designed to kill either juveniles or adults [5]. On the other hand, a harvest strategy that targets both stages in equal proportion (Case $\mathrm{H_e}$) consists of removing all individuals encountered, regardless of their age [4].

We will also assume that the survivorship rates s_a and s_j are related in one of the following manners, which cover the main examples in [4] (see Table 1 there).

$\mathrm{S_1}$: $s_j = 1 - s_a$
$\mathrm{S_e}$: $s_j = s_a$

The former case includes some typical situations in which juvenile survivorship is much lower than adult survivorship (for example, the case $s_j = 0.2$, $s_a = 0.8$ considered in [4]). The latter case assumes that the survivorship rate is the same for juveniles and adults alike.

We emphasize that Case S_1 is sometimes implicitly assumed in the literature. In the absence of harvesting, the system (1)–(2) can be reduced to the second-order difference equation for the size of the adult population

$$A_{n+1} = s_a A_n + s_j \alpha A_{n-1} e^{-\beta A_{n-1}} \tag{3}$$

This equation was introduced by Clark [12, 13] to model whale populations (see also [14–17]). If $\alpha s_j > 1 - s_a$, then Eq. (3) has a positive equilibrium K, which represents the saturation level. This equilibrium satisfies the following equation:

$$s_j \alpha = (1 - s_a) e^{\beta K}, \tag{4}$$

which is sometimes referred to as the *balance equation* [14]. Replacing (4) into (3) gives

$$A_{n+1} = s_a A_n + (1 - s_a) A_{n-1} e^{-\beta(A_{n-1} - K)}$$

This form of Clark's equation, with different choices for g, was used by May [14] and Fisher [15]. See [18–20] for further discussion.

In this paper, we will consider all the six cases that are combinations of the three harvest strategies with the two relations on the survivorship rates listed above, and we will use the above labels to indicate these cases, e.g., "Case H_j–S_1" will refer to the case of juvenile-only harvest in which the survivorship rates are related by the equation $s_j = 1 - s_a$, and "Case S_e" will refer to the three cases in which $s_j = s_a$, taken collectively.

The paper is organized as follows. In Section 2 we apply analytical methods to investigate the existence and stability of equilibrium states of the system as a function of the parameters. We explain the results of this analysis and discuss their biological consequences. In particular, in Section 2.3 we investigate the effect of an increase in population size in spite of an increase in harvesting effort (so-called *hydra effect*), and in Section 2.4 we discuss the phenomenon of destabilization followed by re-stabilization of the population caused by subsequent increases in harvesting (the effect of a *bubble*). Technical proofs of the results of this analysis are postponed to Appendix A. In Section 3 we apply a set-oriented numerical method for the analysis of global dynamics as selected parameters are varied, and we discuss the results of this analysis. In particular, we discuss periodic oscillations, an averaged version of the hydra effect, a numerical counterpart of the bubble effect, as well as synchronous and resonant behavior of the population abundance. Most technical details and remarks are postponed to Appendix B. In Section 4 we briefly compare the results obtained by both methods, and we summarize key findings of our work.

2. Stability analysis of critical points

2.1. Reduction to a single second-order equation

As noticed before for the case without harvesting, the system (1) can be reduced to the Clark model defined by the second-order difference equation for the size of the adult population

$$A_{n+1} = (1-h_a)s_a A_n + (1-h_j)s_j g((1-h_a)A_{n-1}) \tag{5}$$

Consider Eq. (5) with the Ricker map (2). Our first observation is that not all parameters are important for the dynamics. Indeed, the change of variables $x_n = (\beta/r)A_n$, where $r = \ln(\alpha) > 0$, transforms the equation under consideration into

$$x_{n+1} = (1-h_a)s_a x_n + (1-h_j)s_j(1-h_a)x_{n-1}e^{r(1-(1-h_a)x_{n-1})} \tag{6}$$

Since we focus on the changes in the adult population, our aim is to understand the dynamics of this equation, depending on the values of the parameters $h_a, h_j, s_a, s_j \in [0,1]$, and $r > 0$.

Solutions of the difference equation (6) are sequences $\{x_n\}_{n\geq 0}$ that can be obtained by recurrence starting with two nonnegative initial values x_0, x_1. Eq. (6) can be written in the form

$$x_{n+1} = (1-\delta)x_n + pf((1-h_a)x_{n-1})$$

where $f(x) = xe^{r(1-x)}$, $\delta = 1-(1-h_a)s_a$, and $p = (1-h_j)s_j$. Some important aspects of this equation, such as boundedness and persistence, have been studied in [21] and can be applied to Eq. (6). In particular, if $h_a, s_a \in (0,1)$, then all solutions of (6) with $x_0 \geq 0$, $x_1 > 0$, are positive and bounded. Moreover, it follows from [21, Corollary 12] that Eq. (6) is uniformly persistent if $r > r_0$, where

$$r_0 := \ln\left(\frac{1-(1-h_a)s_a}{(1-h_j)(1-h_a)s_j}\right) \tag{7}$$

We recall that the notion of uniform persistence for Eq. (6) means that there is $\varepsilon > 0$ such that $\liminf_{n\to\infty} x_n > \varepsilon$ for every solution $\{x_n\}$ of (6) with positive initial conditions; see, e.g., the recent monograph [22].

2.2. Equilibria of the system

Equilibria provide the most basic information about long-term behavior of solutions, and therefore their existence and stability constitute primary issues to be investigated in any dynamical system. In this section, we investigate this subject with regards to our population model.

A number K is an equilibrium of (6) if and only if it satisfies the equation

$$K = (1-h_a)s_a K + (1-h_j)s_j(1-h_a)Ke^{r(1-(1-h_a)K)} \tag{8}$$

We work with the usual definitions of stability and asymptotic stability (see, e.g., [23, Section 5.3]). In particular, the notions of stability (asymptotic stability) are understood as local stability (local asymptotic stability). We say that the positive equilibrium K is *globally attracting* if it attracts all positive solutions, that is, $\lim_{n\to\infty} x_n = K$ whenever $x_1 > 0$. We say that K is *globally asymptotically stable* if it is asymptotically stable and globally attracting.

The following result provides comprehensive information on the existence and global stability of the equilibria of (6), as well as an actual formula for the equilibrium, which turns out to be unique. The proof of this result is an easy consequence of some results from [21], and can be found in Appendix A.

Proposition 2.1. *Let r_0 be defined by (7). If $r \le r_0$ then the unique equilibrium of (6) is $x = 0$, and all solutions converge to 0. If $r > r_0$ then 0 is unstable and (6) has a unique positive equilibrium*

$$K = \frac{1}{1-h_a}\left(1 - \frac{r_0}{r}\right) \tag{9}$$

Moreover, if $r_0 < r \le r_0 + 1$ then the positive equilibrium K is globally asymptotically stable.

Remark 2.2. An immediate conclusion that can be drawn from Proposition 2.1 is that overharvesting leads to extinction. Moreover, the positive equilibrium K is globally asymptotically stable for harvest rates slightly smaller than the critical value after which the population is doomed to extinction. For example, in Case $\mathrm{H_a}$ the positive equilibrium K is globally asymptotically stable if $h_1^* \le h_a < h_2^*$, and 0 is globally attracting (implying extinction) for $h_a \ge h_2^*$, where

$$h_1^* = 1 - (s_a + (1-h_j)s_j e^{r-1})^{-1}$$
$$h_2^* = 1 - (s_a + (1-h_j)s_j e^{r})^{-1}$$

This remark will be important for the discussion in Section 2.4.

In the following result, proved in Appendix A, we state the stability properties of the positive equilibrium defined by (9) for $r > r_0$.

Proposition 2.3. *Let r_0 be defined by (7). If*

$$r_0 < r < r_0 + \frac{2 - s_a(1-h_a)}{1 - s_a(1-h_a)} \tag{10}$$

then the positive equilibrium K of (6) is locally asymptotically stable. On the other hand, if

$$r > r_0 + \frac{2 - s_a(1-h_a)}{1 - s_a(1-h_a)}$$

then the equilibrium K is unstable.

2.3. The hydra effect

The phenomenon of a seemingly paradoxical increase in population size in response to an increase in per-capita mortality rate was named the *hydra effect* by Abrams and Matsuda (see [1] and references therein) after the mythological beast that grew two heads to replace each that was cut off. Because of its undeniable biological importance, determining situations in which this phenomenon may occur is of great interest; see, e.g., [24]. In [1], Abrams reviewed mechanisms underlying the hydra effect; in particular, this effect may occur in one-dimensional discrete-time generation population models when mortality precedes density dependence. In this section, we begin with a formal definition of what we mean by the hydra effect in our model, and then we answer the question of when this effect occurs.

Definition 2.4. We say that *the hydra effect occurs in the adult population* if Eq. (6) has a stable equilibrium and the equilibrium remains stable and gets larger as the harvest rate is increased.

Since an explicit expression for the equilibrium K is given by (9), it is easy to determine the necessary and sufficient conditions on when K gets larger as the harvesting effort is increased. We state these conditions for the different harvest strategies in our next result, whose proof is postponed to Appendix A.

Proposition 2.5. *In Case* H_{a}*, the hydra effect occurs in the adult population if and only if*

$$r_0 + \frac{1}{1 - s_a(1-h_a)} < r < r_0 + \frac{2 - s_a(1-h_a)}{1 - s_a(1-h_a)} \tag{11}$$

where r_0 *is defined by (7).*

In Cases H_{j} *and* H_{e}*, the hydra effect does not occur in the adult population.*

Proposition 2.5 allows us to plot the values of parameters (h_a, s_a) for which the hydra effect occurs in Eq. (6) for every fixed r in the case of adult-only harvest. In Fig. 1, we do it for $r = 4$ for both cases $\mathrm{H_a}$–$\mathrm{S_1}$ and $\mathrm{H_a}$–$\mathrm{S_e}$.

Notice that Proposition 2.5 yields a result on a stage-specific hydra effect, in which abundance of the adult stage increases with greater adult mortality. We refer to [1] for more comments and related references. We observe that the Hydra effect in the adult population is relatively frequent for low values of the survivorship rate s_j of juveniles. Some numerical results for $s_a = 0.15$, 0.4, and 0.8 are supplied in Table 1.

2.4. Instability due to harvesting and the phenomenon of a bubble

An important question that has attracted attention of ecologists is whether harvesting can lead to population instability or, in other words, if an increase in harvest rates can elevate variability in the abundance of the species under consideration. Indeed, such a phenomenon has been reported in several populations, and one of the more plausible hypotheses that can cause it is the *age*

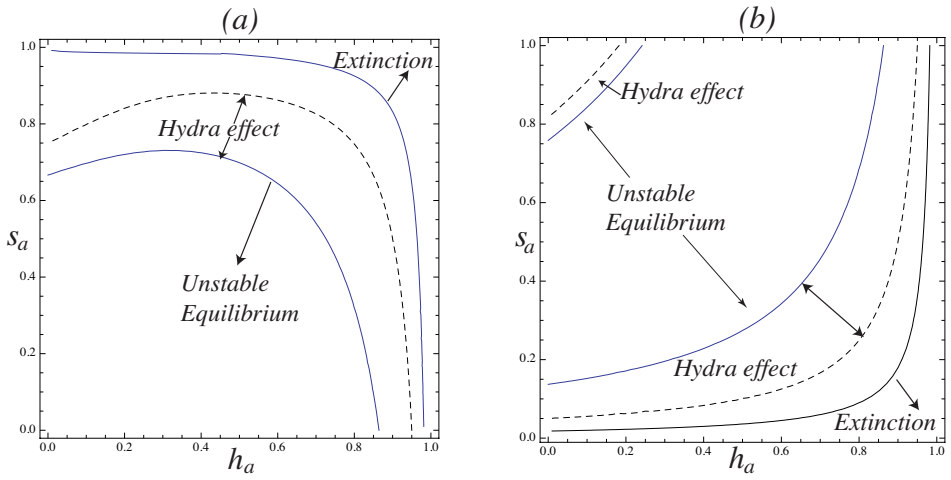

Figure 1: Regions of stability and of the hydra effect in the plane of parameters (h_a, s_a) for Eq. (6) in Case H_a ($h_j = 0$) for $r = 4$. (a) Case H_a–S_1 ($s_j = 1 - s_a$). (b) Case H_a–S_e ($s_j = s_a$).

s_a	Hydra effect in Case S_1	Hydra effect in Case S_e
0.15	$0.841 < h_a < 0.941$	$0.087 < h_a < 0.667$
0.4	$0.7773 < h_a < 0.917$	$0.658 < h_a < 0.875$
0.8	$0.102 < h_a < 0.744$	$0 < h_a < 0.051$ and $0.829 < h_a < 0.937$

Table 1: Ranges of values of the adult harvest rate h_a for which the hydra effect in adult population is observed in Eq. (6) for $r = 4$, Case H_a (adult-only harvest), and different values of s_a. Both Cases: H_a–S_1 ($s_j = 1 - s_a$) and H_a–S_e ($s_j = s_a$), are considered.

truncation effect (see [8, 9], and references therein), as is believed to be the case of fisheries removing large and old individuals through size-age selective fishing. In [4], Zipkin *et al.* argue that population instability as a result of harvesting is possible in the system given by (1) when both fecundity and adult survivorship are high.

Our first result in this direction, which we prove in Appendix A, shows that if adults are not targeted then the positive equilibrium cannot be destabilized as h_j is increased.

Proposition 2.6. *For Eq. (6), in Case H_j, the locally asymptotically stable positive equilibrium cannot be destabilized as h_j is increased.*

Regions of stability in the plane of parameters (h_j, s_a) are shown in Fig. 2. We notice that in Case H_j–S_1 the condition for extinction is independent of the survivorship rate s_a; in this case $r = r_0$ if and only if $h_j = 1 - e^{-r}$ (see the

vertical line $h_j = 1 - e^{-4}$ in Fig. 2(a)).

We also emphasize another fact that is proved in Appendix A. In Case H_j–S_e, if $r \leq 3$ then the equilibrium is asymptotically stable whenever it exists. However, for $r > 3$, increasing mortality of juveniles does stabilize the population for intermediate values of the adult survivorship rate.

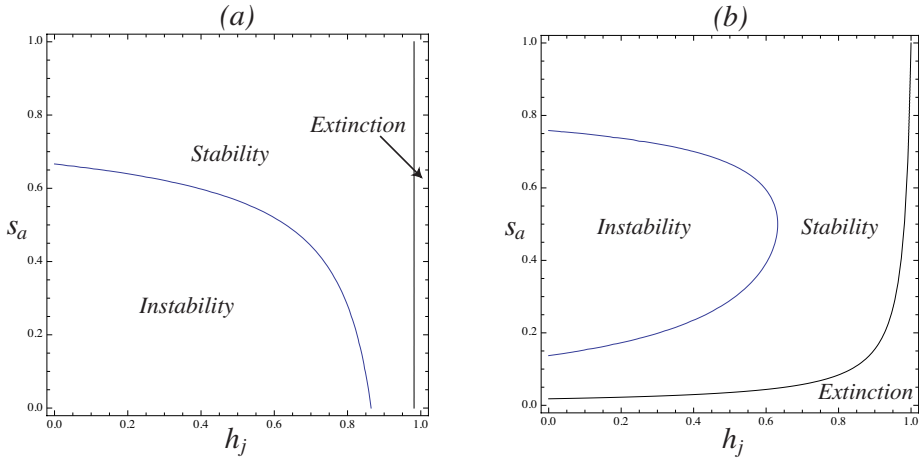

Figure 2: Regions of stability in the plane of parameters (h_j, s_a) for Eq. (6) in Case H_j (juvenile-only harvest, $h_a = 0$) for $r = 4$. (a) Case H_j–S_1 ($s_j = 1 - s_a$). (b) Case H_j–S_e ($s_j = s_a$).

In the remainder of this section, we assume that $h_a > 0$, that is, we consider Cases H_a and H_e. Since, by Proposition 2.1 and Remark 2.2, the positive equilibrium is always globally asymptotically stable for values of h_a slightly smaller than the critical value after which the population is doomed to extinction, one can immediately see that high harvest rates cannot destabilize the equilibrium. Therefore, a mechanism is necessary that allows destabilizing the system and then stabilizing it again. In one-dimensional discrete-time models, this is possible when a period-doubling route to chaos is broken down, giving rise to period-halving bifurcations, which in turn stabilize the system again around an equilibrium point [25, 26]. The bifurcation diagram forms a closed loop-like structure similar to a bubble (see [27, 28]), which gave the name to this phenomenon.

We formalize the idea of destabilizing a population and stabilizing it again by introducing the concept of a *bubble* for Eq. (6), and we provide rigorous analysis of the range of the survivorship parameter s_a for which an increase in the harvest rate h_a of adults leads to the loss and then re-gain of stability.

Definition 2.7. For Eq. (6), we say that *there is a bubble as h_a is increased* if there are points $h_1 < h_2 < h_3$ such that the positive equilibrium of (6) is asymptotically stable for $h_a \in (0, h_1) \cup (h_2, h_3)$, and unstable for $h_a \in (h_1, h_2)$.

The mechanism that destabilizes the positive equilibrium and stabilizes it

again is a Naimark–Sacker bifurcation (see, e.g., [29]). An example is shown in Fig. 3, where we plotted the maximum and minimum values achieved by a solution once the transients have died out.

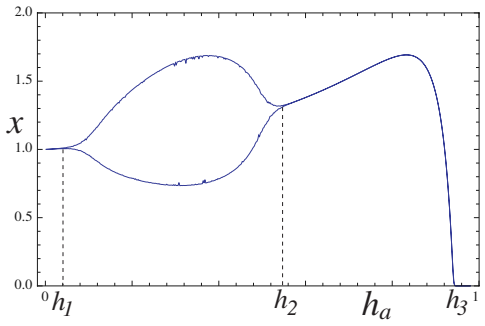

Figure 3: A bubble formed by plotting the minimum and maximum values of a solution of Eq. (6) in Case $\mathrm{H_a}$–$\mathrm{S_1}$ ($h_j = 0$, $s_j = 1 - s_a$), with randomly chosen initial conditions $x_0, x_1 \in [0, 2]$, as h_a is increased, for $r = 4$ and $s_a = 0.7$. We made 200 iterations for each value of h_a, and discarded the first 150. The stable equilibrium is destabilized at h_1 and stabilized again at h_2.

In both Cases $\mathrm{H_a}$ and $\mathrm{H_e}$, the corresponding stability diagrams indicate the existence of a bubble and show the range of values of the survivorship parameter s_a for which a bubble occurs (see Figs. 4 and 6). Actually, analytical results can be derived to determine this range for each given value of the parameter r. In the following result, whose proof can be found in Appendix A, we do this task for Case $\mathrm{H_a}$.

Proposition 2.8. *In Case H_a–S_1, there is a bubble in Eq. (6) as h_a is increased if and only if $r > 3$ and*

$$\frac{r-2}{r-1} < s_a < \frac{e^{r-3}}{1+e^{r-3}} \tag{12}$$

In Case H_a–S_e, there is a bubble in Eq. (6) if and only if $s(r) < s_a \leq 1$, where $s(r)$ is the greatest solution of the equation

$$\ln\left(\frac{1-x}{x}\right) + \frac{1}{1-x} = r - 1 \tag{13}$$

in the interval $(0, 1)$.

The range of values of s_a for which there is a bubble as h_a is increased in Eq. (6) is shown in Fig. 5 for r between 3 and 10 in Cases $\mathrm{H_a}$–$\mathrm{S_1}$ and $\mathrm{H_a}$–$\mathrm{S_e}$. For example, if $r = 4$ then there is a bubble for $s_a \in (2/3, e/(1+e)) \approx (0.66, 0.73)$ in the former case, and for $s_a \in (0.759, 1)$ in the latter.

Remark 2.9. Since $s(r)$ is an increasing function of r, it follows from Proposition 2.8 that the length of the interval of values of the adult survivorship

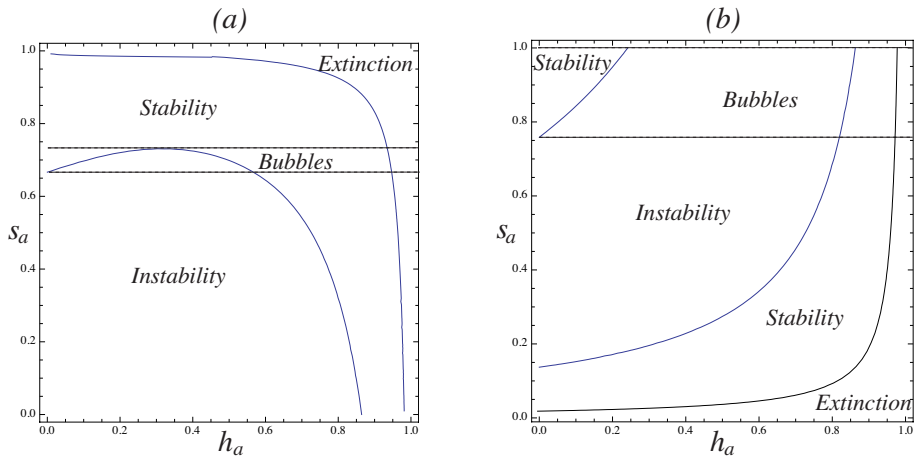

Figure 4: Regions of stability in the plane of parameters (h_a, s_a) for Eq. (6) in Case H_a (adult-only harvest) for $r = 4$. The region where a bubble appears as h_a is increased is delimited by the horizontal dashed lines. (a) Case H_a–S_1 ($s_j = 1 - s_a$). (b) Case H_a–S_e ($s_j = s_a$).

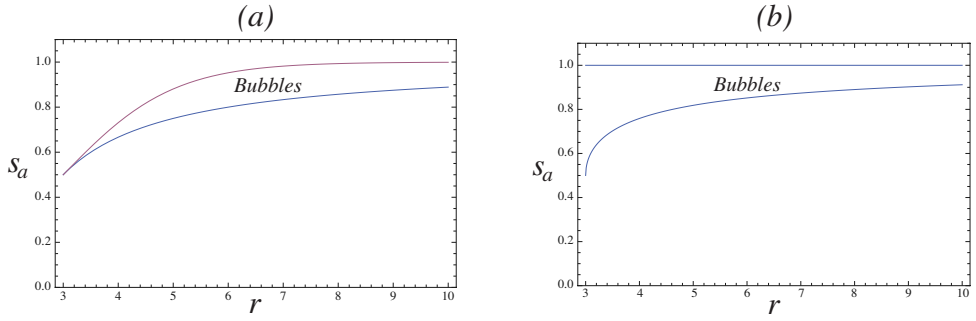

Figure 5: Range of values in the plane of parameters (r, s_a) for which there is a bubble in Eq. (6) as h_a is increased. We consider all the values of $r \in (3, 10)$ in Case H_a (adult-only harvest). (a) Case H_a–S_1 ($s_j = 1 - s_a$). (b) Case H_a–S_e ($s_j = s_a$).

parameter s_a for which there is a bubble as h_a is increased in Eq. (6) is a monotone decreasing function of the parameter r in Case H_a–S_e.

Case H_e reports qualitatively similar results to those of Case H_a, although more intricate calculations are needed. Compare the regions of stability in Fig. 4 with those in Fig. 6.

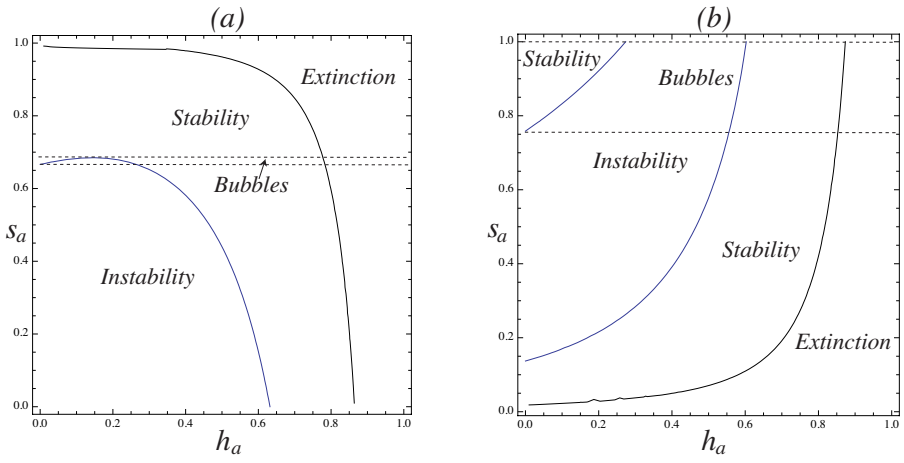

Figure 6: Regions of stability in the plane of parameters (h_a, s_a) for Eq. (6) in Case H_e (equal harvest of adults and juveniles) for $r = 4$. (a) Case H_e–S_1 ($s_j = 1 - s_a$). (b) Case H_e–S_e ($s_j = s_a$).

Existence of a bubble in the bifurcation diagram is a strong indicator of the fact that increasing harvesting can lead to instability in the model, as was observed in recent empirical studies for plant, insect, and fish populations (see [4] and references therein).

Our results are in accordance with the age-truncation hypothesis suggested by Anderson *et al.* [9], who discuss how increased variability in fish abundance may be caused by the fact that fishing typically targets the larger individuals of a species.

We would like to point out that in the literature about discrete-time population models of dimension higher than one, the bubbling phenomenon has been barely treated, although some related diagrams were already obtained for the three dimensional model for the flour beetle *Tribolium* analyzed by Costantino *et al.* [30], and for the model of population dynamics of *Alliaria petiolata* (garlic mustard) recently studied by Pardini *et al.* [10]. Rigorous studies of the phenomenon of bubbling are relatively scarce; for some recent results, see [31].

2.5. Systems with an unstable equilibrium

In the previous sections, we have divided the plane of parameters (h_a, s_a) into different regions depending on the stability properties of the equilibrium, and we have determined the ranges of the parameters for which such phenomena

as the hydra effect and a bubble occur. However, we have not provided any information about the dynamics of the system (1) in the regions where the equilibrium is unstable. It is well known that, even for one-dimensional maps, the asymptotic behavior of solutions can range from simple periodic oscillations to chaos (see, e.g, [32]).

In fact, this remark can provide new conclusions, not raised up by the previous study, regarding the potential of harvesting to increase variability. For example, if we consider Eq. (6) with $r = 4$, Case H_a–S_1, Proposition 2.8 ensures that the equilibrium cannot be destabilized by harvesting for small values of s_a. However, if we look at the bifurcation diagram in Fig. 7 then we see that harvesting indeed enhances variability from a simple four-periodic regime to an apparently chaotic behavior. In Fig. 8, we show time series for 100 generations in the model without harvesting (convergence to a four-periodic regime), and with a rate of harvesting of 60% (apparently chaotic).

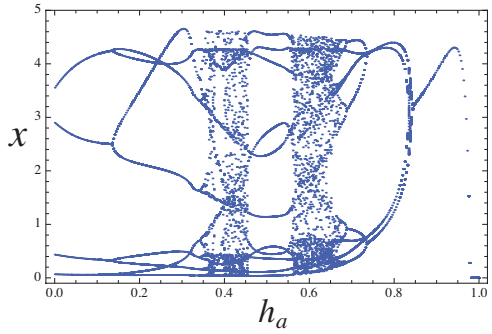

Figure 7: Bifurcation diagram for Eq. (6), Case H_a–S_1, with $r = 4$ and $s_a = 0.15$.

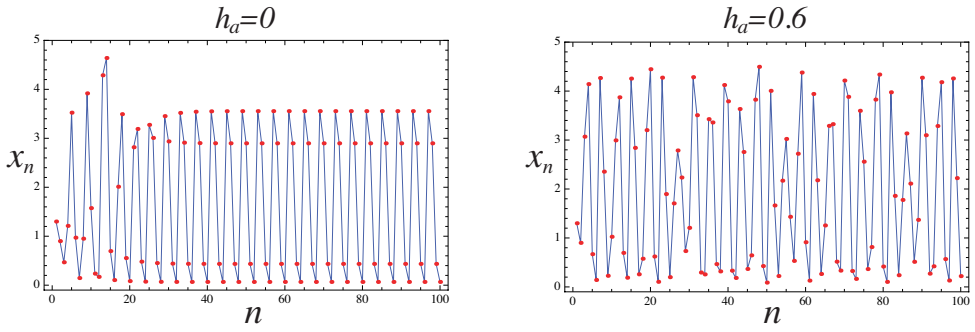

Figure 8: Time series for Eq. (6), Case H_a–S_1, with $r = 4$ and $s_a = 0.15$. Left: without harvesting (a four-periodic attractor is observed); right: with adult harvest rate $h_a = 0.6$ (no periodic pattern appears).

3. Set-oriented numerical analysis of global dynamics

In this section, we apply the method for the analysis of global dynamics introduced in [33], which is based upon rigorous numerical set-oriented computations. This is a computational method that algorithmically subdivides the parameter space into regions of equivalent dynamics, and provides an interactive tool to analyze and visualize, for each specific parameter value, selected features of the dynamics, not only the attractors, but also unstable invariant sets, usually difficult to find using classical methods.

We begin with a brief introduction to this method and we explain how it is applied to our model. Then we describe the results obtained, and we discuss some biologically interesting phenomena that were found with this approach.

3.1. Description of the method

The core idea behind the computational method in question is to decompose the dynamics into isolated invariant sets that correspond to recurrent structures (e.g., fixed points or periodic solutions) in such a way that connecting orbits between them define a strict partial order, like in a gradient system, and then to determine classes of parameters for which these decompositions are equivalent. The computations are carried out using interval arithmetic [34], and the results are mathematically rigorous. This last feature distinguishes our method from approximate numerical simulations, which are typically much cheaper but may not provide reliable results.

The input to the method applied to the system of interest consists of the following data:

(I1) The two-dimensional map defined by (1), with the Ricker map (2), in which we fix $\alpha := e^4$, so that we work with $r = 4$, as discussed in the previous sections, and we also fix the scaling parameter $\beta := \alpha/e$, so that all the solutions with non-negative initial conditions are eventually trapped in $[0, 1]^2$.

(I2) The ranges of the varying parameters. Although the computational method may handle all the parameters h_a, h_j, s_a and s_j varying simultaneously, we limit our attention to two varying parameters at a time, and we consider the six cases listed in Section 1. The first varying parameter is h_a in Case $\mathrm{H_a}$, h_j in Case $\mathrm{H_j}$, and $h_a = h_j$ in Case $\mathrm{H_e}$, and the second varying parameter is s_a, with $s_j = 1 - s_a$ in Case $\mathrm{S_1}$ and $s_j = s_a$ in Case $\mathrm{S_e}$. We vary both parameters from 0 to 1, and thus we take $\Lambda := [0, 1]^2$ for the parameter space.

(I3) The phase space bounding box that contains all asymptotic dynamics, with an additional margin to compensate for numerical overestimates; a quick computation at low resolution suggested that the choice of $B := [0, 1.35]^2$ would be appropriate.

(I4) The resolutions in the parameter space and in the phase space. We subdivide the parameter space Λ uniformly into 500×500 boxes, and the phase space B into 1024×1024 boxes. The choice of the resolutions was made on the basis of the resulting cost of computations, which was between 1,000 and 3,000 CPU hours for each case, with the memory usage not exceeding 2 GB.

The computations run at a computer cluster in a convenient way, using a flexible dynamic parallelization scheme introduced in [35] built into the software.

The output of the computations consists of the following information:

(O1) Classes of parameters for which the qualitative dynamics is equivalent, as computed at the fixed resolution in the phase space by means of a decomposition into chain recurrent components and connecting orbits between them (see Appendix B.1 for a detailed description). These classes are given as subsets of Λ, built of the boxes into which Λ was subdivided.

(O2) For each parameter box, the phase space portrait of the computed outer approximations of the chain recurrent components in terms of isolating neighborhoods, with information on the detected connecting orbits, gathered in a structure called a numerical Morse decomposition, as explained in Appendix B.1. For each of these isolating neighborhoods, the Conley index is computed whenever possible, as explained in Appendix B.2, and also additional quantities are calculated, as discussed in Sections 3.4 and 3.5. Moreover, each isolating neighborhood is classified either as *attracting* or *unstable*. Additionally, based on the Conley index, the neighborhood may be said to be *of the type* of a certain hyperbolic fixed point or hyperbolic periodic orbit (in particular, it may be called *repelling*), as explained in Appendix B.2

3.2. Results of the computations

In Fig. 9, continuation diagrams computed for the six cases under consideration are shown. Each continuation class consisting of more than 1 element is indicated in some solid color, with colors repeated for small classes that are at some distance from each other. A few largest classes were given labels (a), (b), etc., and are briefly discussed below. The reader is invited to explore the details at the interactive presentation provided at the website [36]. The classes corresponding to the labels (a), (b), etc., will be denoted below $\mathcal{C}_a$, $\mathcal{C}_b$, etc.

The three subcases of Case S_1, grouped in the left column in Fig. 9, show similar dynamics to each other, so we limit the detailed discussion to Case H_a–S_1. The classes that appear in the other two cases are labeled in a consistent way so that they represent similar dynamics to the one that was found in the corresponding classes in the case discussed.

For parameters in $\mathcal{C}_a$, a small isolating neighborhood of the origin is attracting, and it has been verified rigorously that no other recurrent dynamics is present in B, and thus the neighborhood of the origin contains a global attractor.

As the parameters in $\mathcal{C}_a$ get closer to the border with $\mathcal{C}_b$, the neighborhood gets stretched, and it splits upon entering $\mathcal{C}_b$ into an unstable neighborhood of the origin and another attracting isolating neighborhood. The latter neighborhood gets farther apart from the origin if one changes the parameters towards the middle of $\mathcal{C}_b$.

As the parameters in $\mathcal{C}_b$ change towards the border with $\mathcal{C}_c$, the attracting neighborhood gets larger, and in $\mathcal{C}_c$ this neighborhood gets split into a pair formed by a small round repelling neighborhood surrounded by an attracting neighborhood in the shape of a ring, as shown in Fig. 10(a). For parameters in

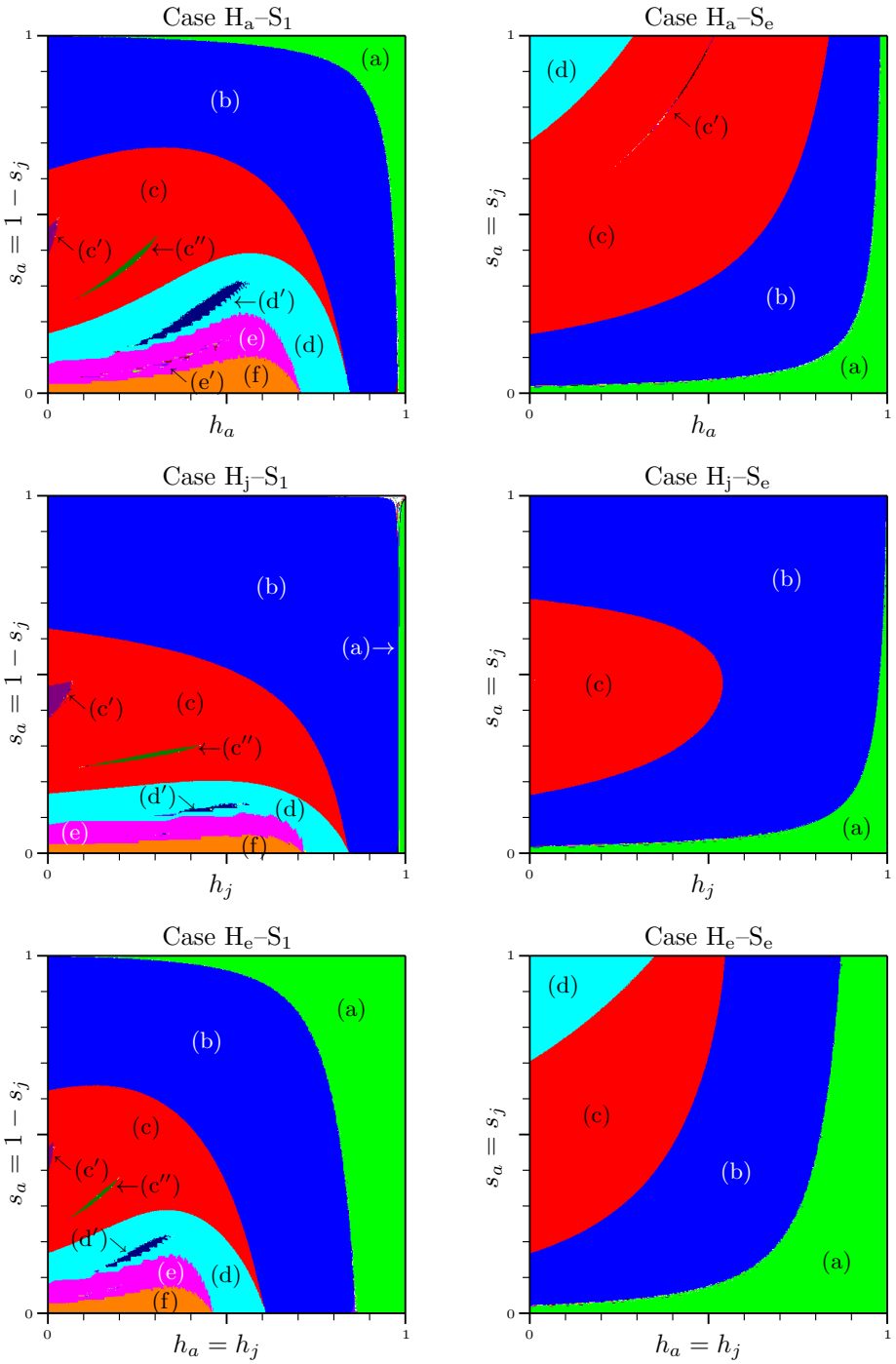

Figure 9: Continuation diagrams for the six cases considered in Section 3, with $r = 4$ fixed. Classes of equivalent dynamics are indicated with shades of grey (colors online). Selected continuation classes are given labels, and the global dynamics found in each of them is discussed in the text.

$\mathcal{C}_{c'}$ and $\mathcal{C}_{c''}$, the attracting ring is split into a pair of two isolating neighborhoods of the type of an attracting and saddle periodic orbit, respectively, of period 5 (in $\mathcal{C}_{c'}$) or 9 (in $\mathcal{C}_{c''}$); these sets are illustrated in Figs. 10(b) and 10(c), respectively.

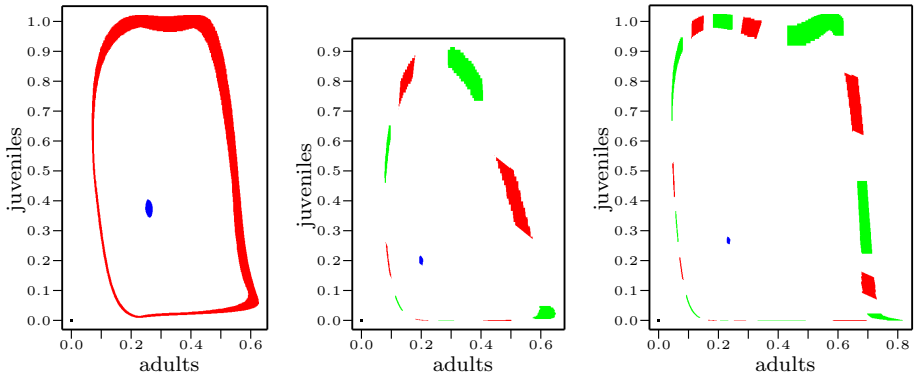

Figure 10: Some saddle-node configurations found in Case H_a–S_1. (a) An attracting isolating neighborhood in the shape of a ring observed in Class $\mathcal{C}_c$, with a repeller inside the ring. (b) The ring split into a pair of attracting (dark grey, red online) and saddle-like (bright grey, green online) five-periodic neighborhoods observed in Class $\mathcal{C}_{c'}$. (c) The ring split into a pair of attracting (dark grey, red online) and saddle-like (bright grey, green online) nine-periodic neighborhoods observed in Class $\mathcal{C}_{c''}$. The corresponding parameter boxes are: (a) $(200, 263)$: $[0.400, 0.402] \times [0.526, 0.528]$, (b) $(3, 223)$: $[0.006, 0.008] \times [0.446, 0.448]$, (c) $(118, 185)$: $[0.236, 0.238] \times [0.370, 0.372]$.

For parameters in $\mathcal{C}_d$, the invariant ring described above is split into a pair of neighborhoods of the type of four-periodic orbits, an attracting one and a saddle one, as shown in Fig. 11(a). In $\mathcal{C}_{d'}$, the attracting neighborhood is split even further, like in a period-doubling bifurcation, as illustrated in Fig. 11(b).

As the parameters in $\mathcal{C}_d$ are changed towards the border with $\mathcal{C}_e$, the four-periodic attracting neighborhood gets larger, and is eventually replaced in $\mathcal{C}_e$ with a thick attracting ring surrounding the small repelling neighborhood in the middle, as shown in Fig. 12(a). In some small regions of parameters labeled with (e′), inside this thick ring, a four-periodic repeller is visible, as illustrated in Fig. 12(b). It looks like a neighborhood of an unstable periodic orbit embedded in a chaotic attractor.

Eventually, for parameters in $\mathcal{C}_f$, a single huge attracting isolating neighborhood is observed (not shown here), which apparently indicates complicated recurrent dynamics taking place in that region of the phase space, or at least the lack of or very weak hyperbolicity of solutions, which makes it impossible to separate various recurrent pieces (if any) at the resolution at which the computations are done.

In addition to all this, in the narrow regions of parameters along the bottom edge of the diagram, one can also see periodic isolating neighborhoods formed along the coordinate axes (unless a single huge isolating neighborhood is found

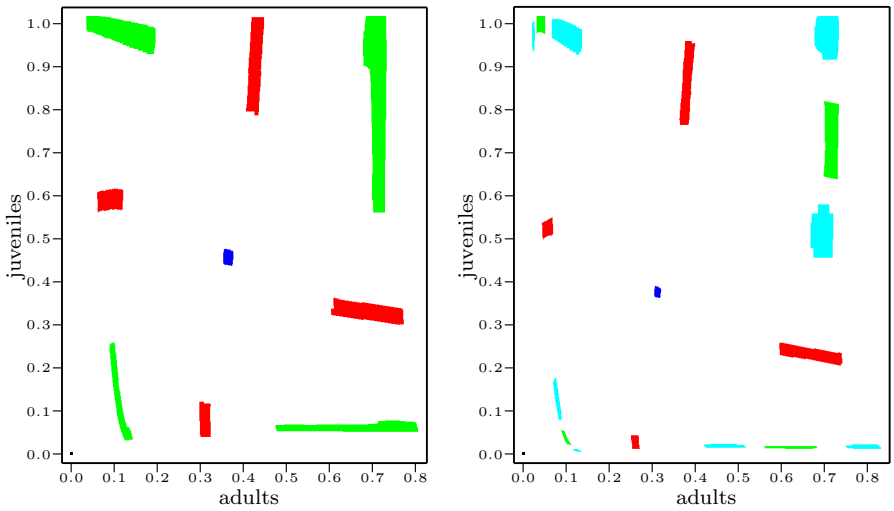

Figure 11: A period doubling bifurcation observed in Case H_a–S_1. (a) A numerical Morse decomposition observed in Class $\mathcal{C}_d$. In addition to an unstable neighborhood of the origin (black) and a repelling isolating neighborhood in the center of the picture (grey, blue online), a pair of saddle-type (dark grey, red online) and attracting (light grey, green online) four-periodic isolating neighborhoods are present. (b) In Class $\mathcal{C}_{d'}$, the attracting four-periodic isolating neighborhood is replaced by a saddle-type four-periodic neighborhood (darker light grey, green online) coupled with an eight-periodic attracting neighborhood (brighter light grey, cyan online). The corresponding parameter boxes are: (a) $(307, 144)$: $[0.614, 0.618] \times [0.288, 0.290]$, (b) $(251, 144)$: $[0.502, 0.504] \times [0.288, 0.290]$.

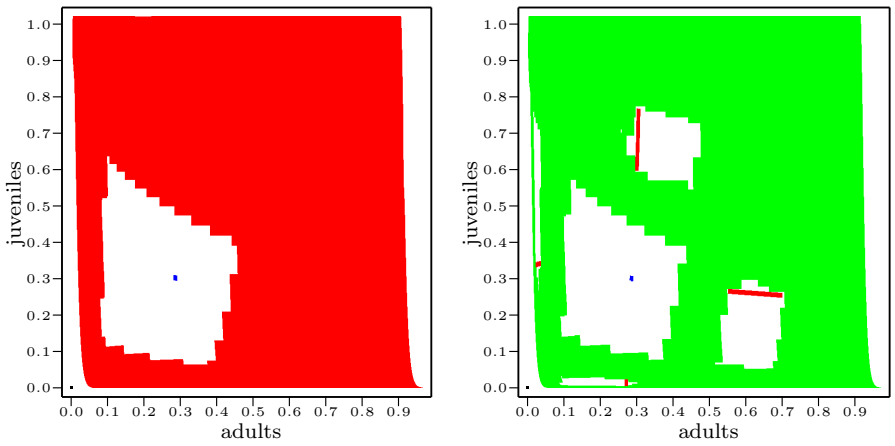

Figure 12: Large isolating neighborhoods observed in Case H_a–S_1: (a) A large attracting isolating neighborhood in the shape of a thick ring (grey, red online), with a repelling isolating neighborhood in the center (dark grey, blue online), in addition to an unstable neighborhood of the origin (black), observed in Class $\mathcal{C}_e$. (b) A repelling four-periodic isolating neighborhood (dark grey, red online) revealing additional details on the structure of the thick ring (grey, green online) in Class $\mathcal{C}_{e'}$. The corresponding parameter boxes are: (a) $(201, 60)$: $[0.402, 0.404] \times [0.120, 0.122]$, (b) $(201, 55)$: $[0.402, 0.404] \times [0.110, 0.112]$.

that touches the axes, as it happens for smaller harvest rates). Moreover, these neighborhoods resemble shadows of the other isolating neighborhoods which are of unusually regular shape and form a checkered pattern (see Fig. 13). We discuss these particular configurations in Section 3.6.

Similarly to Case S_1, the three subcases of Case S_e exhibit global dynamics similar to each other, except the five-periodic orbit observed in Class $\mathcal{C}_{c'}$ was only found in Case H_a–S_e. (It is not ruled out that some five-periodic windows may also exist in the other cases, but they were not detected at the resolution at which the computations were carried out.) As in the former case, the classes in the three diagrams are labeled in a consistent way, following the type of dynamics encountered.

For parameters in $\mathcal{C}_a$, a small attracting neighborhood of the origin is the only recurrent dynamics found. For parameters in $\mathcal{C}_b$, this neighborhood is split into a small unstable neighborhood of the origin and a small attracting neighborhood located at some distance from the origin. This attracting neighborhood gets larger and in the region $\mathcal{C}_c$ eventually splits into a small repelling neighborhood surrounded by an attracting neighborhood in the shape of a ring, as shown in Fig. 14(a). In some small areas of parameters labeled by $\mathcal{C}_{c'}$ in Case H_a–S_e, this ring is split into a pair of five-periodic attracting and saddle-type neighborhoods, as illustrated in Fig. 14(b). For parameters in $\mathcal{C}_d$, the attracting ring and the small repelling neighborhood inside have collided, and a single attracting neighborhood is observed (not shown).

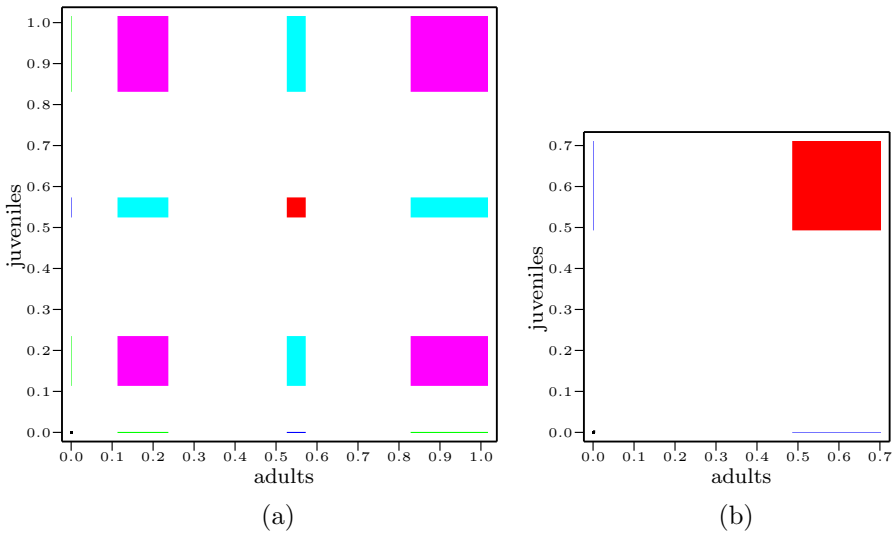

Figure 13: Numerical Morse decompositions that form checkered patterns (resonance) and contain (very thin) isolating neighborhoods along the coordinate axes (synchronization), observed in Case H_a–S_1 for very low values of s_a. The corresponding parameter boxes are: (a) $(385, 0)$: $[0.770, 0.772] \times [0.000, 0.002]$, (b) $(487, 7)$: $[0.974, 0.976] \times [0.014, 0.016]$.

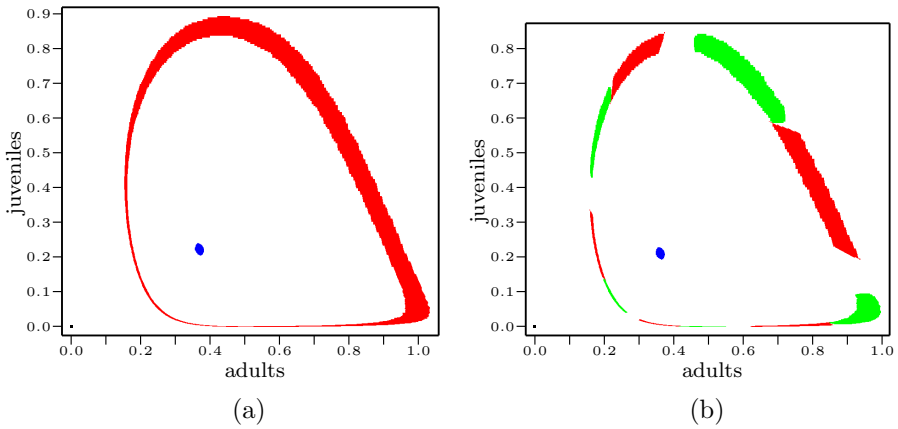

Figure 14: A saddle-node configuration found in Case H_a–S_e: (a) An attracting isolating neighborhood in the shape of a ring, with a small repelling neighborhood in the center, observed in Class $\mathcal{C}_c$. (b) The ring split into a pair of five-periodic saddle-type (dark grey, red online) and attracting (light grey, green online) neighborhoods, observed in Class $\mathcal{C}_{c'}$. The corresponding parameter boxes are: (a) $(240, 445)$: $[0.480, 0.482] \times [0.890, 0.892]$, (b) $(230, 445)$: $[0.460, 0.462] \times [0.890, 0.892]$.

Summarizing, we were able to compute a comprehensive overview of global dynamics for the entire ranges of the two varying parameters in each of the six cases of interest. The richness of the dynamics that we observe suggests that the resolution of our computations is satisfactory, and the results we obtained are meaningful. Since the resolutions we chose in the parameters and in the phase space are at the border of precision at which these quantities can be controlled or determined for a real biological system, possible additional details that might be revealed at finer resolutions would be of negligible biological importance. The reader is referred to [37] for a more in-depth discussion of this issue and for a suggestion of a theory that deals with dynamics perceived at finite resolution.

Some specific phenomena found using the computational method are discussed in the subsequent sections.

3.3. Periodic attractors

Periodic behavior of a system is nearly as important as an equilibrium state. Although the population state is not constant at a periodic cycle, it repeats with a regular periodicity, and thus corresponds to predictable oscillations in population abundance.

The results of the computations described in Section 3.2 reveal the presence of several continuation classes in which isolating neighborhoods corresponding to periodic cycles were found, many of them being attracting, often in a configuration with an isolating neighborhood of a saddle type. Some of these instances are plotted in Figs. 10, 11, and 14.

In some cases periodic behavior may be found in a large continuation class, like Class (d) in Case H_a–S_1 (see Figs. 9 and 11). However, periodic behavior also appears in some smaller classes that look like isles inside a larger class, in which an isolating neighborhood in the shape of a ring is observed instead. This phenomenon of breaking recurrent dynamics into a pair of unstable and stable periodic cycles is of special biological importance, because it suggests a breakdown of seemingly chaotic behavior into a well predictable repetitive cycle.

Windows of attracting periodic orbits in bifurcation diagrams were previously found in other discrete-time biological models such as the two-dimensional nonlinear Leslie model investigated by Guckenheimer *et al.* [38], the two-dimensional Maynard Smith delayed model for growth population studied by Aronson *et al.* [39], and the three-dimensional model for the dynamics of the flour beetle *Tribolium* considered by Costantino *et al.* [30, 40]. For Clark's delayed recruitment model with Ricker-type nonlinearity, this phenomenon was observed numerically by Botsford *et al.* as the parameter r was increased [16, 17, 41]. However, we would like to point out that saddle-node configurations such as those observed in Figs. 10, 11, and 14 are very difficult to detect using classical approaches.

Saddle-node configurations are common in higher dimensional dynamical models in an ecological context, and a typical effect is that trajectories starting near the stable manifold of a saddle will initially move towards the saddle before moving away along a hyperbolic orbit towards its ultimate attractor (see

Cushing *et al.* [42] and references therein). As a consequence, transients in the time series data are usually longer for some initial population sizes.

3.4. The averaged hydra effect

Although it is much more difficult to prove the occurrence of the hydra effect using the results discussed in this section, one can detect some indications of such an effect by means of the analysis of certain properties of attracting isolating neighborhoods.

We cannot measure the adult population size at an equilibrium point, as we did in Section 2.3, because we simply do not have well identified fixed points. Therefore, we choose to analyze the average adult population size computed for an entire isolating neighborhood instead. As a consequence, we talk about the *averaged hydra effect*.

Note that due to the linear scale in the variables and thanks to the uniform grid in the phase space, the average adult population size in N can be easily computed with good accuracy by summing the adult population sizes corresponding to the centers of all the boxes that form N, and then dividing the result by the number of boxes in N.

In our computations, exactly one attracting neighborhood was found for each parameter box.[1] This simplifies the situation considerably, because if there had existed multiple attracting isolating neighborhoods then we would have had to consider the evolution of each of these sets separately as harvest rate is increased, with all the subtleties coming from possible bifurcations of the isolating neighborhoods.

The core feature of the hydra effect is the increase in the adult population size in spite of an increase in harvest rate. This kind of an effect can be perceived in a situation in which the attracting neighborhood is replaced by one that has a greater average adult population size, as the harvest rate increases. We refer to Appendix B.3 for a formal definition of the averaged hydra effect, as well as for the definition of the *size* and *relative size* of this effect.

The average size of the adult population computed for Cases H_a–S_1 and H_a–S_e at each parameter box under consideration is illustrated in Figs. 15(a) and 16(a), respectively, and the boxes for which considerable averaged hydra effect was found are indicated in Figs. 15(b) and 16(b). Results for the remaining cases are only shown at the website [36]. Very limited amount of hydra effect (of relative size up to 25%) was found in Case H_j–S_1, and no hydra effect exceeding 10% was found in Case H_j–S_e, which agrees with Proposition 2.5. In Case H_e–S_1, very small parameter regions with the averaged hydra effect of relative size up to 38% were found. However, in Case H_e–S_e, considerable hydra effect

[1] Actually, in most cases in which the attracting isolating neighborhood was touching the coordinate axes, the numerical calculations did not prove that its image was contained in its interior, because of the points whose one of the coordinates was 0. However, we know that for this model, the region B absorbs every positive orbit, so the isolating neighborhood that is a minimal element with respect to the partial order constructed for the numerical Morse decomposition, is in fact attracting.

was found in the region of low harvest rate and high survival rate, approximately corresponding to the region (d) in Fig. 9 for the same case.

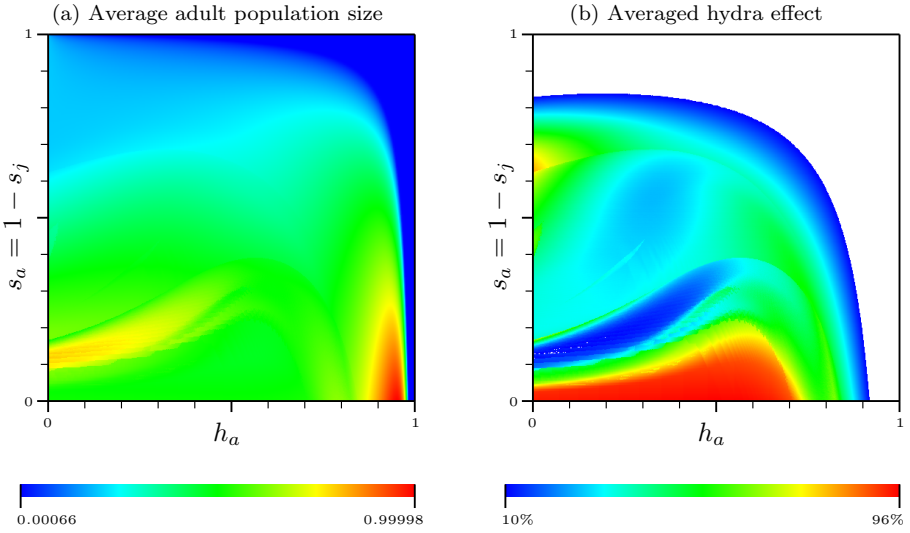

Figure 15: Numerical investigation of the averaged hydra effect in Case H_a–S_1: (a) The average size of the adult population for attracting neighborhoods computed at each parameter box. The size is illustrated with colors according to the scale plotted below the image. (b) Parameters for which the averaged hydra effect of relative size at least 10% was found, with color indicating the relative size of this effect.

The hydra effect found in Case H_e–S_e seemingly contradicts the analytical results obtained in Section 2.3. However, the reason for this difference, as well as for some other discrepancies between the analytical and numerical results, is the fact that different definitions of hydra effect are used in both cases. While in Proposition 2.5 an immediate increase in the adult popluation size represented by the stable positive equilibrium was considered only, here we take into account the entire attracting isolating neighborhood, independent of what it contains, and we look at *any* increase in harvest rate, possibly a very large one. As a consequence, an increase in the average adult population size observed in a model may be simply due to weaker stability of the equilibrium in the direction in which the adult population is larger, or to the fact that an isolating neighborhood for another stable solution (a periodic orbit, for instance) observed for some higher harvest rate (possibly a much higher one), where the equilibrium is no longer stable, results in a higher average adult population size. Indeed, all these cases are very much relevant from the biological point of view, because a real system modeled by the equations may be subject to small distortions, which are then all accounted for in this approach. Moreover, the knowledge of a possibility of hydra effect that occurs after a considerable increase in harvest rate only may be important in practice, for instance, in the case of pest control, where application of an insecticide increases mortality in a radical manner.

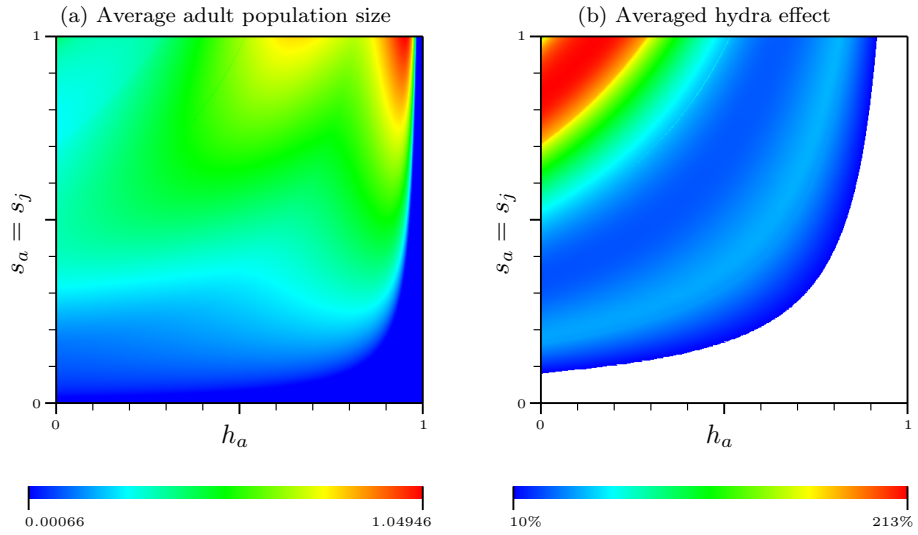

Figure 16: Numerical investigation of the averaged hydra effect in Case H_a–S_e: (a) The average size of the adult population for attracting neighborhoods computed at each parameter box. The size is illustrated with colors according to the scale plotted below the image. (The value greater than 1 is due to numerical overestimates.) (b) Parameters for which the averaged hydra effect of relative size at least 10% was found, with color indicating the relative size of this effect.

Although numerical investigation of the hydra effect in the region of instability was already done before for one-dimensional models depending on one parameter [1, 43], as far as we are aware, our work has been the first time that this task was carried out in a 2-parameter setting.

3.5. Population size fluctuations and the numerical bubble effect

The isolating neighborhoods are constructed as components of recurrent dynamics, and thus they are transitive at the resolution at which the computations are carried out. In other words, within the given accuracy, a transition of population from each state is not ruled out to any other state within the same isolating neighborhood. This either corresponds to the existence of some exact trajectories of the modeled system (1) from each state to the other, or some trajectories with small perturbations (within the accuracy of computations) on the way.

Since an attracting neighborhood does not allow trajectories to escape, the dynamics inside such a neighborhood corresponds to a long-term behavior of a population. Such dynamics can either be very simple, e.g., a periodic or almost periodic orbit, or may have complicated fine structures, e.g., a chaotic attractor. Nevertheless, the entire attracting neighborhood reflects all the possible configurations that can be reached by the population in its evolution over time.

It is natural to use the size of an attracting neighborhood as a means of measuring how much population size can fluctuate, especially that this is a

global attractor in our case. Note that fluctuations in population size measured in this way reflect changes in all the age groups, not just the total population size, nor the adult population size alone.

The fact that our model exhibits exactly one attracting isolating neighborhood simplifies the definitions and the discussion greatly (see discussion on this issue in Section 3.4 and Footnote 1).

By verifying how the size of the attracting neighborhood changes upon increase in harvest rate, one can determine how harvesting contributes to stabilization or destabilization of the population. If this quantity increases as harvest rate is increased, and then decreases down to or below the previous value as harvest rate is further increased then we encounter a phenomenon analogous to a bubble, as discussed in Section 2.4.

Since obviously the population stabilizes trivially as harvest rate is increased to 1, we are only interested in the effect of a bubble if the average adult population size in the attracting neighborhood after stabilization is comparable to the average adult population size in the attracting neighborhood before the destabilization.

We refer to Appendix B.4 for a formal definition of the numerical bubble effect which we suggest for this analysis, as well as for the definition of the *size* and *relative size* of this effect.

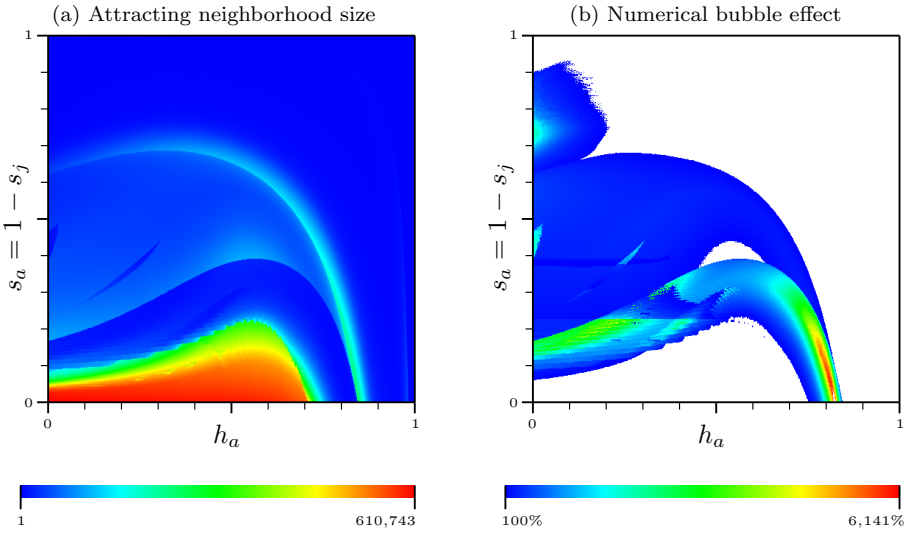

Figure 17: Numerical investigation of population size fluctuations in Case H_a–S_1: (a) The size of the attracting neighborhood (in boxes), indicated according to the color scale shown below the image. (b) Parameters for which the numerical bubble effect of relative size greater than 100% was found and the average adult population size after the stabilization did not drop below 75% of the original size, with color indicating the size of this effect. The top value of 6,141%, corresponds to an over 61-fold increase in the attracting neighborhood size.

The size of the attracting neighborhood computed for Cases H_a–S_1 and

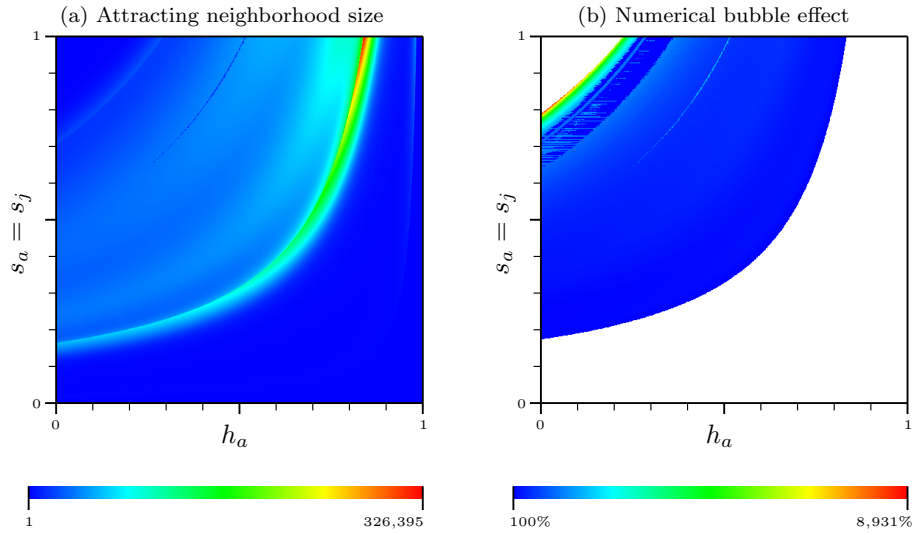

Figure 18: Numerical investigation of population size fluctuations in Case H_a–S_e: (a) The size of the attracting neighborhood (in boxes), indicated according to the color scale shown below the image. (b) Parameters for which the numerical bubble effect of relative size greater than 100% was found and the average adult population size after the stabilization did not drop below 75% of the original size, with color indicating the size of this effect. The top value of 8,931% corresponds to a nearly 90-fold increase in the attracting neighborhood size.

H_a–S_e at each parameter box under consideration is illustrated in Figs. 17(a) and 18(a), respectively, and the parameters for which the numerical bubble effect was found are indicated in Figs. 17(b) and 18(b). Results for the remaining cases are only shown at the website [36].

In most situations, the numerical bubble effect was found when an attractor that co-exists with one or more unstable isolating neighborhoods collides with them to become a large attractor, which in turn gradually decreases in size as harvest rate is increased. This scenario explains the existence of the numerical bubble effect in Case H_j, where no bubble effect concerning the equilibrium takes place, as stated in Proposition 2.6.

The "classical" bubble effect that agrees with the scenario outlined in Section 2.4 was observed in Cases H_a–S_e and H_e–S_e in the top 1/3 area of the diagram, approximately. However, for the parameters in the top left corner, no numerical bubble effect was spotted due to the fact that the re-gained stability of the equilibrium is weaker, which results in the size of the isolating neighborhood staying above the original one.

The disagreements found between the analytical and numerical results are due to the differences in the definitions. First of all, Definition 2.7 is stated for a fixed parameter s_a and takes into consideration the entire range of all harvest rates possible. As a consequence, the regions in which the analytically found bubble effect occurs are marked as horizontal stripes in Figs. 4 and 6.

The numerical bubble effect, on the contrary, is defined for each parameter point (h_a, s_a) or (h_j, s_a) separately, and considers harvest rates limited to those higher than h_a (or h_j, respectively). Therefore, regions of parameters for which a numerical bubble effect was found have more complicated shapes than those coming from the analytical calculations. Secondly, instead of considering the existence of a stable positive equilibrium, the numerical bubble effect is based upon the size of the attracting neighborhood, which depends on many factors, including the "strength" of stability of the stable equilibrium whenever it exists.

3.6. Synchronization and resonance

The phenomenon of presence of exactly one age class of a population at a time is called *synchronization*. It indicates that the age transitions of all individuals are synchronized across the entire population, thus the name. This phenomenon is mathematically characterized by an orbit whose points have exactly one positive coordinate, which is then called a *synchronous orbit*. Synchronous phenomena are observed in some natural insect populations, for example, if there is a single reproductive age class and the adults die after having laid eggs. Periodical cicadas, inhabiting the eastern United States, are typical examples of such a case [44]. A question as to whether a given model admits synchronous orbits has recently drawn some attention due to its biological importance; see, e.g., [45, 46].

If $s_a = 0$ then the system (1) simplifies to

$$\begin{aligned} A_{n+1} &= (1 - h_j)s_j J_n \\ J_{n+1} &= g((1 - h_a)A_n) \end{aligned} \tag{14}$$

and thus Eq. (5) for the adult population size becomes

$$A_{n+1} = (1 - h_j)s_j g((1 - h_a)A_{n-1}) \tag{15}$$

If $\{k_j\}$, $\{l_j\}$, $j = 1, 3, 5, \ldots$, are periodic solutions (including fixed points) of Eq. (15) then the interlaced periodic orbit $\{k_1, l_1, k_3, l_3, k_5, l_5, \ldots\}$ is also a solution of (15). Since in our model $g(0) = 0$, the trivial orbit $l_j \equiv 0$ is also a solution to (15), which can be combined with a non-zero fixed point or a non-trivial periodic orbit of (15), if any, and give rise to a synchronous periodic orbit. This explains the existence of the periodic isolating neighborhoods located along the boundary of the positive cone for low values of s_a, including those in Fig. 13.

Alongside with the synchronous orbits, in the same phase space diagrams, one can also see orbits created by other combinations of periodic solutions of (15), which also inherit the stability of those periodic solutions in the corresponding directions. Such orbits very much resemble the phenomenon of *resonance* between age classes, and was studied, e.g., in [47, see Fig. 1].

4. Conclusions and final remarks

Recent theoretical and empirical studies have revealed that an induced increase in mortality in a population may lead to unexpected and sometimes

undesirable consequences. On the one hand, the phenomenon of an increase in population abundance in response to an increase in mortality (the hydra effect) shows that control efforts of nuisance and invasive species require careful consideration [1, 3, 4] and a good understanding of the underlying population dynamics [10]. On the other hand, fishing or harvesting strategies should take into account the possibility of increasing variability in population abundance, thus leading to elevated complexity of the dynamics and the risk of extinction [4, 8–10, 40].

Since the presence of these phenomena, as well as their strength, depends strongly on the relevant parameters of the model (survivorship rates of the different age classes, growth rates) and the harvesting strategies, a thorough characterization of the dynamics in response to an increase in mortality is necessary. The main aim of this paper was to address this task for a simple stage-structured discrete-time population model proposed in [4], considering different harvesting strategies, depending on a selection of the classes of individuals from the population to be targeted.

The two substantially different methodologies that were applied to the analysis of the population model under consideration have provided a comprehensive overview of the dynamics of the system. The results obtained with these methods complement each other, and they agree on most of the overlapping part.

We rigorously analyzed the hydra effect, understood as an increase in population size represented by a stable equilibrium in response to an increase in the harvest rate. The analytical approach to this question in the parameter ranges where there exists a stable equilibrium was complemented by approximate numerical computation of the parameter ranges for which the averaged hydra effect occurs.

Moreover, we rigorously proved that increasing adult mortality can produce a bubble, defined as a destabilization and re-stabilization of the positive equilibrium upon subsequent increases in the harvest rate. We also proved that this scenario is not possible in the strategy of juvenile-only mortality. We studied an analogous phenomenon in the numerical context, and we found parameters for which an increase in the fluctuations of population size occurs as a result of increased harvesting, followed by a return to the original value upon further harvesting increase. We found and discussed some differences from the results of the analytical study.

Additionally, the numerical method provided information about attracting periodic cycles appearing in some parameter ranges of unstable positive equilibrium.

As a general conclusion regarding the methodology of investigation of dynamics, we have demonstrated that although the importance of the analytical approach is undeniable and provides rigorous results about equilibria of the system, it turns out that using modern numerical methods may provide considerable amount of additional information, in part rigorous (like the computed decompositions of the phase space) and in part heuristic (like the averaged hydra effect and the numerical bubble effect).

We remark that the results obtained in Section 2 can be seen as a rigorous

analysis of the effects of harvesting in the dynamics of the celebrated delayed Clark model [12, 13] used in fisheries.

Regarding the implications of our study in fisheries management and in control of plagues, some words of caution are in order. In particular, our study of the averaged hydra effect in Section 3.4 shows that the average of the population size is greater for values of the harvest rate close to the border of collapse, especially if adult survivorship rates are low. This conclusion is in agreement with previous results for other population models [1, 7, 43], and strongly indicates that the possibility of the hydra effect must not be used to justify greater fishing. Another implication of the counterintuitive effects of harvesting discussed in this paper is that, in control of plagues, culling may not be effective until removal rates are very high [4, 10].

Acknowledgements

The work of both authors was partially supported by the Spanish Ministry of Science and Innovation and FEDER, grant MTM2010-14837. Moreover, the work of P. Pilarczyk was additionally supported in part from Fundo Europeu de Desenvolvimento Regional (FEDER) through COMPETE—Programa Operacional Factores de Competitividade (POFC) and from the Portuguese National Funds through Fundação para a Ciência e a Tecnologia (FCT) in the framework of the research projects FCOMP-01-0124-FEDER-010645 (ref. FCT PTDC/MAT/098871/2008) and Est-C/MAT/UI0013/2011, as well as from the Research Center of Mathematics of the University of Minho through the FCT Pluriannual Funding Program.

The authors thank K. Mischaikow's lab at Rutgers University (supported in part by NSF, DoE, DARPA, and AFOSR) and the Computer Science and Technology Center at Departamento de Informática of Universidade do Minho for providing their cluster computing facilities.

Finally, the authors express their gratitude to the anonymous reviewers for their insightful critique and helpful suggestions.

Statements required in the *Guide for Authors*

For this paper, E. Liz chose the subject and conducted the analysis of stability of equilibria using analytical methods (Sections 2 and Appendix A), P. Pilarczyk did the numerical analysis of global dynamics using software of his authorship (Sections 3 and Appendix B), and both authors organized the material and edited the paper together.

None of the sponsors listed in the Acknowledgements section had any influence on study design, analysis and interpretation of data, nor the decision to submit the manuscript for publication.

Appendix A. Proofs of propositions in Section 2

This section gathers the technical proofs of the results of the analysis conducted in Section 2.

Appendix A.1. Proof of Proposition 2.1

We will apply some results from [21]. To do that, let us observe that Eq. (6) can be written in the form

$$x_{n+1} = (1-\delta)x_n + px_{n-1}f_1(x_{n-1})$$

where $f_1(x) = (1-h_a)e^{r(1-(1-h_a)x)}$, $\delta = 1-(1-h_a)s_a$, and $p = (1-h_j)s_j$.

Thus, condition $r \leq r_0$ is equivalent to $pf_1(0) \leq \delta$. Since f_1 is strictly decreasing on $(0,\infty)$, Corollary 12 in [21] ensures that all solutions of (6) converge to 0 if $r \leq r_0$.

Since $K \neq 0$ is a solution of (8) if and only if $(1-h_a)K = 1-r_0/r$, it is clear that there exists a unique positive solution K of (8) if and only if $r > r_0$, and the expression of K is given by (9). On the other hand, Corollary 10 in [21] states that K is globally asymptotically stable if $F'(K) \geq 0$, where $F(x) = xf_1(x)$. Since $F'(x) \geq 0$ if and only if $x \in [0, 1/(r(1-h_a))]$, we get that

$$F'(K) \geq 0 \Longleftrightarrow (1-h_a)K \leq \frac{1}{r}$$

Since, by (6), $(1-h_a)K = 1-r_0/r$, it follows that

$$F'(K) \geq 0 \Longleftrightarrow 1-\frac{r_0}{r} \leq \frac{1}{r} \Longleftrightarrow r - r_0 \leq 1 \Longleftrightarrow r \leq r_0 + 1$$

□

Appendix A.2. Proof of Proposition 2.3

The linearized equation of (6) about $x = K$ is

$$y_{n+1} = (1-h_a)s_a y_n + (1-h_j)s_j(1-h_a)f'((1-h_a)K)y_{n-1} \tag{A.1}$$

where $f(x) = xe^{r(1-x)}$. Hence, the associated characteristic equation is

$$q(y) = y^2 - (1-h_a)s_a y - (1-h_j)s_j(1-h_a)f'((1-h_a)K) = 0$$

In view of Proposition 2.1, we can restrict ourselves to the case $f'((1-h_a)K) < 0$. It is easy to check that all roots of $q(x)$ remain in the interior of the unit disk if and only if $b < 1$, where

$$b = -(1-h_j)s_j(1-h_a)f'((1-h_a)K) > 0$$

Direct computations show that $b < 1$ if and only if the second inequality in (10) holds. We recall that the first one is necessary to ensure the existence of K. The conclusion of Proposition 2.3 follows from the linearized stability result (see, e.g., [23, Theorem 5.15]). □

Appendix A.3. Proof of Proposition 2.5.

The first inequality in (11) is equivalent to the condition $\partial K/\partial h_a > 0$ in Case $\mathrm{H_a}$, while the second inequality is the necessary condition for the asymptotic stability of K.

In Case $\mathrm{H_e}$, the condition $\partial K/\partial h_a > 0$ leads to

$$r > r_0 + \frac{2 - s_a(1-h_a)}{1 - s_a(1-h_a)}$$

But this means that K is unstable. Thus, there is no observable hydra effect in the adult population.

Finally, in Case $\mathrm{H_j}$, $\partial K/\partial h_j = -1/(r(1-h_j)) < 0$, so an increase in harvesting always leads to a decrease in the size of the equilibrium K. □

Appendix A.4. Proof of Proposition 2.6

By Proposition 2.3, we know that, for a fixed $r > r_0$, the positive equilibrium K of (6) changes its asymptotic stability when

$$r = r_0 + \frac{2 - s_a(1-h_a)}{1 - s_a(1-h_a)} \tag{A.2}$$

where, since $h_a = 0$, r_0 is defined as

$$r_0 = \ln\left(\frac{1-s_a}{(1-h_j)s_j}\right)$$

Thus, the border of the asymptotic stability region is given by the equation

$$r = \ln\left(\frac{1-s_a}{(1-h_j)s_j}\right) + \frac{2-s_a}{1-s_a} \tag{A.3}$$

In Case $\mathrm{S_1}$, Eq. (A.3) simplifies to

$$\frac{2-s_a}{1-s_a} = r + \ln(1-h_j)$$

This equation allows us to obtain the explicit expression

$$s_a = 1 - \frac{1}{r - 1 + \ln(1-h_j)} := \Sigma(h_j)$$

so that K is unstable if $s_a < \Sigma(h_j)$ and it is asymptotically stable if $s_a > \Sigma(h_j)$. Since

$$\frac{\partial \Sigma}{\partial h_j} = \frac{-(1-s_a)^2}{1-h_j} < 0$$

increasing h_j cannot destabilize a stable equilibrium K. See Fig. 2 (a).

Now consider Case $\mathrm{S_e}$ ($s_j = s_a$). Eq. (A.3) becomes

$$r = \frac{2-s_a}{1-s_a} + \ln\left(\frac{1-s_a}{(1-h_j)s_a}\right)$$

This equation defines h_j as a function of s_a in an explicit form:

$$h_j = H(s_a) = 1 - \frac{1-s_a}{s_a} e^{1-r+1/(1-s_a)} \tag{A.4}$$

It is easy to check that the function H has a unique critical point in $(0,1)$ at $s_a = 1/2$, which is a local maximum. Since

$$H(1/2) = 1 - e^{3-r} > 0 \Longleftrightarrow r > 3$$

it follows that the positive equilibrium K is asymptotically stable whenever it exists (i.e., $r_0 < r$) if $r \leq 3$. If $r > 3$, then K is asymptotically stable if $h_j > H(s_a)$, and is unstable if $h_j < H(s_a)$, where $H(s_a)$ was defined in (A.4). This means that the positive equilibrium cannot be destabilized as h_j is increased; actually, an increase in harvesting of juveniles tends to stabilize the positive equilibrium (see Fig. 2 (b)). □

Appendix A.5. Proof of Proposition 2.8

As in the proof of Proposition 2.6, recall that, for a fixed $r > r_0$, the positive equilibrium K of (6) changes its asymptotic stability when (A.2) holds.

Let us consider the function

$$G(s_a, h_a) = \frac{2 - s_a(1-h_a)}{1 - s_a(1-h_a)} + r_0 - r \tag{A.5}$$

An application of the Implicit Function Theorem allows us to ensure that Eq. (A.2) defines s_a as a smooth function of h_a and

$$s_a'(h_a) = -\frac{\partial G/\partial h_a}{\partial G/\partial s_a} \tag{A.6}$$

Let us begin with the proof of Case H_a–S_1. In this case,

$$r_0 = \ln\left(\frac{1-(1-h_a)s_a}{(1-h_a)(1-s_a)}\right)$$

and (A.2) becomes

$$\frac{2 - s_a(1-h_a)}{1 - s_a(1-h_a)} + \ln\left(\frac{1-(1-h_a)s_a}{(1-h_a)(1-s_a)}\right) = r \tag{A.7}$$

We first prove that, for every fixed $h_a \in [0,1)$, there exists at most one value of $s_a \in [0,1]$ for which (A.7) holds. Indeed, let us fix $h_a \in [0,1)$ We introduce the variable $z = 1 - s_a(1-h_a)$, $s_a \in [0,1]$. With this notation, (A.7) is equivalent to

$$g_1(z) := \frac{1}{z} + \ln\left(\frac{z}{z-h_a}\right) = r - 1 \tag{A.8}$$

Since

$$g_1'(z) = \frac{-1}{z^2} + \frac{1}{z} - \frac{1}{z-h_a}$$

and $0 < z - h_a \leq z$, it follows that g_1 is decreasing on $(0, 1]$. It is hence clear that Eq. (A.8) has at most one solution $z(h_a)$. Therefore, there is at most one solution of (A.7) given by

$$s_a(h_a) = \frac{1 - z(h_a)}{1 - h_a}$$

We notice that, for $h_a = 0$, this solution exists and it is given by

$$s_a(0) = 1 - z(0) = 1 - \frac{1}{r-1} = \frac{r-2}{r-1}$$

On the other hand, (A.6) leads to

$$s_a'(h_a) = \frac{(1 - s_a)\,(2(1 - h_a)s_a - 1)}{(1 - h_a)(1 - s_a) + (1 - h_a)s_a h_a^2}$$

The denominator of this fraction is always positive, and hence $s_a'(h_a) < 0$ if and only if $2s_a(1 - h_a) < 1$.

In particular, $s_a'(0) \leq 0$ implies that $s_a'(h_a) < 0$ for all $h_a \in (0, 1)$. In this case, there is no bubble, because s_a is a one-to-one function of h_a. Thus we need $s_a'(0) > 0$, which is equivalent to $s_a(0) > 1/2$. Notice that $s_a(h_a)$ is always decreasing at $h_a = 1 - e^{2-r}$, since this corresponds to the case $s_a = 0$, and then

$$s_a'(1 - e^{2-r}) = \frac{-1}{(1 - h_a)} < 0$$

Since $s_a'(h_a) = 0$ only if $h_a = \bar{h_a} := 1 - 1/(2s_a)$, the curve $s_a(h_a)$ is unimodal when $s_a(0) > 1/2$. This means that there are two points where the stability of K changes if and only if $s_a \in (S_1(r), S_2(r))$, where

$$S_1(r) = s_a(0) = \frac{r-2}{r-1}$$

$$S_2(r) = s_a(\bar{h_a}) = \frac{e^{r-3}}{1 + e^{r-3}}$$

To complete the proof, we notice that a necessary condition for the existence of a bubble is $s_a(0) > 1/2$, which is equivalent to $r > 3$.

Next consider Case $\mathrm{H_a}$–$\mathrm{S_e}$. The expression (A.2) turns into

$$\frac{2 - s_a(1 - h_a)}{1 - s_a(1 - h_a)} + \ln\left(\frac{1 - (1 - h_a)s_a}{(1 - h_a)s_a}\right) = r \tag{A.9}$$

As in the previous case, we study the number of possible solutions of (A.9) for every fixed $h_a \in [0, 1)$. In this case, the change of variables $z = 1 - s_a(1 - h_a)$ transforms (A.9) into

$$g_2(z) := \frac{1}{z} + \ln\left(\frac{z}{1 - z}\right) = r - 1 \tag{A.10}$$

Since $g_2'(z) = (2z-1)/(z^2(1-z))$, it follows that $g_2'(z) < 0$ for $z \in (0, 1/2)$, $g_2'(z) > 0$ for $z \in (1/2, 1)$, and there is a global minimum $g_2(1/2) = 2$. Moreover, $\lim_{z\to 0^+} g_2(z) = \lim_{z\to 1^-} g_2(z) = \infty$. Thus, (A.10) has two solutions $z_1(h_a)$, $z_2(h_a)$ in $(0, 1)$ if $r > 3$, and no solution if $r < 3$. Therefore, for $r > 3$, Eq. (A.9) has at most two solutions

$$s_i(h_a) = \frac{1 - z_i(h_a)}{1 - h_a},\ i = 1, 2$$

For $h_a = 0$, these solutions exist and are defined by $s_i(0) = 1 - z_i(0)$, $i = 1, 2$. Notice that $s_1(0), s_2(0)$ are the solutions of (13) in $(0, 1)$.

Next consider (A.6), which, after simplification, boils down to

$$s_a'(h_a) = \frac{s_a}{1 - h_a} \tag{A.11}$$

Thus, it follows that s_a is an increasing function of h_a. Moreover, its simple expression allows us to integrate (A.11) and obtain

$$s_a(h_a) = \frac{s_a(0)}{1 - h_a}$$

Hence, for every $r > 3$, the solutions of Eq. (A.9) in $[0, 1] \times [0, 1]$ are defined by the two increasing curves

$$s_1(h_a) = \frac{s_1(0)}{1 - h_a}$$
$$s_2(h_a) = \frac{s_2(0)}{1 - h_a}$$

where $s_1(0) < s_2(0)$ are the solutions of (13) in $(0, 1)$.

Notice that

$$s_i(h_a) = 1 \iff s_i(0) = 1 - h_a \iff h_a = 1 - s_i(0) \in (0, 1)$$

for $i = 1, 2$. It follows that the graphs of s_1 and s_2 intersect the line $s_a = 1$ before leaving the square $[0, 1] \times [0, 1]$. Therefore, it is clear that there is a bubble as h_a is increased if and only if $r > 3$ and $s_a \in (s_2(0), 1]$. See Fig. A.19 for a representation of the graphs of $s_1(h_a)$ and $s_2(h_a)$ in the case $r = 4$. □

Appendix B. Technical details and remarks for Section 3

This appendix gathers various technical details of and remarks on the computational method used in Section 3, as well as some notes on the interpretation of the results of the computations.

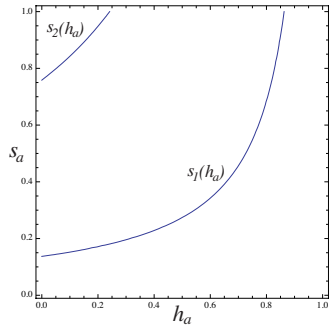

Figure A.19: Illustration for the proof of Proposition 2.6: Boundaries of the region of stability for Eq. (6) with $r = 4$, $h_j = 0$ and $s_j = s_a$.

Appendix B.1. Technical description of the numerical method

In this section we introduce the definitions and terminology necessary to explain the numerical method applied in Section 3.

Let $f\colon X \to X$ be a continuous map on a topological space X. A set $S \subset X$ is an *invariant set* with respect to f if $f(S) = S$. The *invariant part* of a set $N \subset X$ is $\mathrm{Inv}N := \bigcup\{S \subset N : f(S) = S\}$. The set N is called an *isolating neighborhood* if N is compact and $\mathrm{Inv}N \subset \mathrm{int}N$, where $\mathrm{int}N$ denotes the interior of N. S is an *isolated invariant set* if $S = \mathrm{Inv}N$ for some isolating neighborhood N.

Any sequence $\{x_k\}_{k\in\mathbb{Z}}$ of points $x_k \in X$ such that $f(x_k) = x_{k+1}$ is called a *complete orbit* (or just an *orbit* for short). An analogous sequence indexed by the non-negative integers only is called a *positive orbit*.

A *Morse decomposition* (see [48]) of X with respect to f is a finite collection of disjoint isolated invariant sets (called *Morse sets*) $S_1, \ldots, S_p$ with a strict partial ordering $\prec$ on the index set $\{1, \ldots, p\}$ such that for every $x \in X \setminus (S_1 \cup \cdots \cup S_p)$ and for every complete orbit $\{\gamma_k\}_{k\in\mathbb{Z}}$ such that $\gamma_0 = x$ there exist indices $i \prec j$ such that $\gamma_k \to S_i$ as $k \to \infty$ and $\gamma_k \to S_j$ as $k \to -\infty$.

A *rectangular set* is a product of compact intervals. Given a rectangular set $R = [a_1, a_1 + \delta_1] \times \cdots \times [a_n, a_n + \delta_n] \subset \mathbb{R}^n$ and integer numbers $s_1, \ldots, s_n > 0$, we call the following set an $s_1 \times \cdots \times s_n$ *uniform rectangular grid in* R:

$$\mathcal{G}_{s_1,\ldots,s_n}(R) := \Bigg\{ \prod_{i=1}^{n} [a_i + \frac{j_i}{s_i}\delta_i, a_i + \frac{j_i+1}{s_i}\delta_i] : \\ j_i \in \{0, \ldots, s_i - 1\}, i \in \{1, \ldots, n\} \Bigg\}$$

The individual boxes in the grid are referred to by the n-tuples $(j_1, \ldots, j_n)$ for convenience.

Consider an m-parameter family of maps on $\mathbb{R}^n$:

$$f\colon \mathbb{R}^n \times \mathbb{R}^m \ni (x, \lambda) \mapsto f_\lambda(x) \in \mathbb{R}^n \tag{B.1}$$

Let $B \subset \mathbb{R}^n$ and $\Lambda \subset \mathbb{R}^m$ be rectangular sets.

Let $d_1, \ldots, d_n > 0$ and $s_1, \ldots, s_m > 0$ be integer numbers, taken in our computations as $d_1 := d_2 := 2^{10} = 1024$ (with $n = 2$) and $s_1 := s_2 := 500$ (with $m = 2$). In the computational method introduced in [33], for each parameter box $L \subset \Lambda$ in the $s_1 \times \cdots \times s_m$ uniform rectangular grid in Λ, a rigorous outer estimate of the map f_λ valid for all the parameters $\lambda \in L$ is automatically computed using interval arithmetic, on each of the boxes in the $d_1 \times \cdots \times d_n$ uniform rectangular grid in B. Then a family of sets $N_1, \ldots, N_p \subset B$ is constructed with some ordering $\prec$ on $\{1, \ldots, p\}$, such that for each $\lambda \in L$, each set N_i, $i = 1, \ldots, p$, is an isolating neighborhood in B, and whenever a possibility of the existence of an orbit from N_i to N_j is detected, the relation $N_j \prec N_i$ is set. The family $\{S_i := \mathrm{Inv} N_i : i = 1, \ldots, p\}$ forms a Morse decomposition of $\mathrm{Inv} B$ with respect to f_λ with the ordering $\prec$. The sets N_i are constructed as unions of closed boxes with respect to the $d_1 \times \cdots \times d_n$ uniform rectangular grid in B. The collection $N_1, \ldots, N_p$ is called a *numerical Morse decomposition*, and the isolating neighborhoods $N_1, \ldots, N_p$ are called *numerical Morse sets*.

A numerical Morse decomposition can be schematically depicted as a directed graph whose vertices correspond to the Morse sets and edges indicate possible connecting orbits between them. In order to simplify such a representation, one can plot the transitive reduction of this graph, as is done in the presentation of the results at [36].

Appendix B.2. The Conley index

The *Conley index*, introduced by Conley [48] for flows, and generalized, e.g., by Mrozek [49] and Szymczak [50] to discrete semidynamical systems induced by continuous maps, is a topological invariant that provides information about isolated invariant sets. Its homological version is algorithmically computable (to certain extent) from an isolating neighborhood and an outer estimate of the map, like those described in Appendix B.1, and is thus useful in this type of computations. This index takes into account the *exit set* of an isolating neighborhood N, which is the closure of $f(N) \setminus N$, and thus reflects the stability of what N contains.

The definition of the homological Conley index is based upon an index pair, and, roughly speaking, consists of the relative homology of the index pair, as well as the map induced in relative homology, further called the *index map*. This data may be represented as a finite sequence of finitely generated groups, e.g., $(\mathbb{Z}, 0, \mathbb{Z}^2)$, together with the images of homology generators by the index map, expressed as combinations of homology generators, at each level of gradation separately. Since the actual Conley index involves additional reduction (or otherwise it depends on the index pair instead of being an invariant of the isolated invariant set), and the reduced canonical form seems to be very hard to compute, the non-zero eigenvalues of the index map may be used as a simplified and reliable invariant.

For each isolating neighborhood N computed with the method described in Appendix B.1, an index pair can be easily constructed by taking N and the part of the forward image of N which sticks out of N, provided that this

image and also its further image are both fully contained in the phase space B. Otherwise, it is unknown whether N is an isolating neighborhood in $\mathbb{R}^n$, and then the Conley index cannot be computed. This situation typically happens if N is too close to the boundary of B. For example, in our computations it was the case each time with the neighborhood of the origin, and also with the synchronous orbits discussed in Section 3.6 (see also Fig. 13).

The knowledge of the Conley index of an isolating neighborhood N allows to draw conclusions on the invariant part of N. In particular, if the index of N is nontrivial then $\mathrm{Inv}N \neq \emptyset$. The index can also be used to prove the existence of periodic orbits or more complicated dynamics.

For the purpose of this paper, the Conley index and the relation of $f(N)$ with respect to N is used in order to classify each computed isolating neighborhood N on the basis of stability. We say that an isolating neighborhood N is *attracting* if $f(N) \subset N$, that is, if the image of N is entirely contained in N. One can prove that then N contains a local attractor, which justifies this terminology. Otherwise, if the image of N is not fully contained in N, we say that N is *unstable*. If N has the Conley index of a hyperbolic fixed point or a hyperbolic periodic orbit with d-dimensional unstable manifold then we say that N *is of the type* of the corresponding point or orbit. For a typical system, it is likely that N indeed contains a periodic orbit of the expected period, but—since the Conley index is a purely topological tool and does not provide information about derivatives—the actual stability of such an orbit may be different, and the dynamics in N may turn out to be much more complicated than seen from outside (that is, from the perspective of the isolating neighborhood). If $N \subset \mathbb{R}^n$ is of the type of a fixed point or a periodic orbit with n-dimensional unstable manifold then we say that N is *repelling*.

Since detailed introduction to the Conley index is beyond the scope of this paper and requires certain knowledge of algebraic topology, we refer the reader to [48–50] for more details on the Conley index, and to [51, 52] and references therein for discussion of some technical aspects of the computation of this index in the way in which it was implemented in the software used in Section 3. Brief explanation on how to interpret the information on the Conley indices of isolating neighborhoods in the online presentation [36] of the results can also be found in [33].

Appendix B.3. Definition of the averaged hydra effect

The definition of the averaged hydra effect discussed in Section 3.4 can be formalized as follows.

Let $i \in \{1, \ldots, m\}$ be an index of a harvest rate parameter in the system (B.1). Let $\lambda = (\lambda_1, \ldots, \lambda_m) \in \mathbb{R}^m$. We say that the system (B.1) experiences the *averaged hydra effect at resolution* $\mathcal{R}$ *at the parameter* λ *as* λ_i *is increased* if the average adult population size p in the attracting neighborhood N computed at a parameter box b containing λ is smaller than the average adult population size p' in the attracting neighborhood N' computed for another parameter box b' containing $\lambda' = (\lambda_1, \ldots, \lambda'_i, \ldots, \lambda_m)$, where $\lambda'_i > \lambda_i$, provided that the numerical

Morse decomposition computed at the parameter box b and at b' has a unique attracting neighborhood.

The maximal difference $p'-p$ over all valid λ' and the corresponding quotient $(p'-p)/p$ are called, respectively, the *size* and the *relative size* of the averaged hydra effect.

Appendix B.4. Definition of the numerical bubble effect

The definition of the numerical bubble effect discussed in Section 3.5 can be formalized as follows.

Let $i \in \{1,\dots,m\}$ be an index of a harvest rate parameter in the system (B.1). Let $\lambda = (\lambda_1,\dots,\lambda_m) \in \mathbb{R}^m$. We say that the adult population in the system (B.1) experiences the *numerical bubble effect at resolution $\mathcal{R}$ at the parameter λ as λ_i is increased* if the volume v of the attracting neighborhood N computed at a parameter box b containing λ is smaller than the volume v' of the attracting neighborhood N' computed for another parameter box b' containing $\lambda' = (\lambda_1,\dots,\lambda_i',\dots,\lambda_m)$, where $\lambda_i' > \lambda_i$, and greater than or equal to the volume v'' of the attracting neighborhood N'' computed for yet another parameter box b'' containing $\lambda'' = (\lambda_1,\dots,\lambda_i'',\dots,\lambda_m)$, where $\lambda_i'' > \lambda_i'$, provided that the numerical Morse decomposition computed at each of the parameter boxes b, b' and b'' has a unique attracting neighborhood, and additionally the average adult population size p'' in N'' is at least as large as a certain percentage of the average adult population size p in N (the actual percentage threshold depends on a particular application, and we set it to 75% for the model considered in this paper).

The maximal difference $v'-v$ over all valid pairs (λ',λ'') and the corresponding quotient $(v'-v)/v$ are called, respectively, the *size* and the *relative size* of the numerical bubble effect.

References

[1] P.A. Abrams, When does greater mortality increase population size? The long story and diverse mechanisms underlying the hydra effect, Ecol. Lett. 12 (2009) 462–474.

[2] A.M. De Roos, T. Schellekens, T. Van Kooten, K. Van De Wolfshaar, D. Claessen, L. Persson, Food-dependent growth leads to overcompensation in stage-specific biomass when mortality increases: the influence of maturation versus reproduction regulation, Am. Nat. 170 (2007) E59–E76.

[3] E.F. Zipkin, P.J. Sullivan, E.G. Cooch, C.E. Kraft, B.J. Shuter, B.C. Weidel, Overcompensatory response of a smallmouth bass (Micropterus dolomieu) population to harvest: release from competition? Can. Fish. Aquat. Sci. 65 (2008) 2279–2292.

[4] E.F. Zipkin, C.E. Kraft, E.G. Cooch, P.J. Sullivan, When can efforts to control nuisance and invasive species backfire? Ecol. Appl. 19 (2009) 1585–1595.

[5] A.J. Terry, S.A. Gourley, Perverse consequences of infrequently culling a pest, Bull. Math. Biol. 72 (2010) 1666–1695.

[6] J.R. Beddington, R.M. May, Harvesting natural populations in a randomly fluctuating environment, Science 197 (1977) 463–465.

[7] P.A. Abrams, C. Quince, The impact of mortality in a predator population size and stability in sytems with stage-structured prey, Theor. Popul. Biol. 68 (2005) 253–266.

[8] C.H. Hsieh, C.S. Reiss, J.R. Hunter, J.R. Beddington, R.M. May, G. Sugihara, Fishing elevates variability in the abundance of exploited species, Nature 443 (2006) 859–862.

[9] C.N.K. Anderson, C.H. Hsieh, S.A. Sandin, R. Hewitt, A. Hollowed, J. Beddington, R.M. May, G. Sugihara, Why fishing magnifies fluctuations in fish abundance, Nature 452 (2008) 835–839.

[10] E.A. Pardini, J.M. Drake, J.M. Chase, T.M. Knight, Complex population dynamics and control of the invasive biennial *Alliaria petiolata* (garlic mustard), Ecol. Appl. 19 (2009) 387–397.

[11] W.E. Ricker, Stock and recruitment, J. Fish. Res. Bd. Can. 11 (1954) 559–623.

[12] C.W. Clark, A delayed recruitment model of population dynamics with an application to baleen whale populations, J. Math. Biol. 3 (1976) 381–391.

[13] C.W. Clark, Mathematical Bioeconomics: The Optimal Management of Renewable Resources, second ed., John Wiley & Sons, Hoboken, New Jersey, 1990.

[14] R.M. May, Mathematical models in whaling and fisheries management, in: G.F. Oster (ed.), Some mathematical questions in biology, Amer. Math. Soc., Providence, R.I., 1980, pp. 1–64.

[15] M.E. Fisher, Stability of a class of delay–difference equations, Nonlinear Anal. 8 (1984) 645–654.

[16] L.W. Botsford, Further analysis of Clark's delayed recruitment model, Bull. Math. Biol. 54 (1992) 275–293.

[17] K. Higgins, A. Hastings, L.W. Botsford, Density dependence and age structure: Nonlinear dynamics and population behavior, Am. Nat. 149 (1997) 247–269.

[18] H.A. El-Morshedy, E. Liz, Globally attracting fixed points in higher order discrete population models, J. Math. Biol. 53 (2006) 365–384.

[19] H.A. El-Morshedy, V. Jiménez López, E. Liz, Periodic points and stability in Clark's delayed recruitment model, Nonlinear Anal., Real World Appl. 9 (2008) 776–790.

[20] E. Liz, Complex dynamics of survival and extinction in simple population models with harvesting, Theor. Ecol. 3 (2010) 209–221.

[21] I. Győri, S. Trofimchuk, Global attractivity and persistence in a discrete population model, J. Differ. Equations Appl. 6 (2000) 647–665.

[22] H.L. Smith, H.R. Thieme, Dynamical Systems and Population Persistence, Amer. Math. Soc., Providence, R.I., 2011.

[23] S. Elaydi, An Introduction to Difference Equations, 3rd ed., Springer Verlag, New York, 2005.

[24] M. Sieber, F. Hilker The hydra effect in predator-prey models, J. Math. Biol. (2011), DOI: 10.1007/s00285-011-0416-6.

[25] H.E. Nusse, J.A. Yorke, Period halving for $x_{n+1} = MF(x_n)$ where F has negative Schwarzian derivative. Phys. Lett. A 127 (1988) 328–334.

[26] L. Stone, Period-doubling reversals and chaos in simple ecological models, Nature 365 (1993) 617–620.

[27] G. Ambika, N.V. Sujatha, Bubbling and bistability in two parameter discrete systems, Pramana—J. Phys. 54 (2000) 751–761.

[28] M. Bier, T.C. Bountis, Remerging Feigenbaum trees in dynamical systems, Phys. Lett. A 104 (1984) 239–244.

[29] S. Wiggins, Introduction to applied nonlinear dynamical systems and chaos, Springer-Verlag, New York, 1990.

[30] R.F. Costantino, J.M. Cushing, B. Dennis, R.A. Desharnais, Experimentally induced transitions in the dynamic behaviour of insect populations, Nature 375 (1995) 227–230.

[31] E. Sander, J.A. Yorke, Period-doubling cascades galore, Ergodic Theory Dynam. Systems 31 (2011) 1249–1267.

[32] R.M. May, Simple mathematical models with very complicated dynamics, Nature 261 (1976) 459–467.

[33] Z. Arai, W. Kalies, H. Kokubu, K. Mischaikow, H. Oka, P. Pilarczyk, A database schema for the analysis of global dynamics of multiparameter systems, SIAM J. Appl. Dyn. Syst. 8 (2009) 757–789.

[34] R.E. Moore, Interval analysis, Prentice-Hall, Inc., Englewood Cliffs, N.J., 1966.

[35] P. Pilarczyk, Parallelization method for a continuous property, Foundations of Computational Mathematics 10 (2010) 93–114.

[36] P. Pilarczyk, A stage-structured discrete population model with harvesting. Results of computations, `http://www.pawelpilarczyk.com/harvesting/` (2011).

[37] S. Luzzatto, P. Pilarczyk, Finite resolution dynamics, Foundations of Computational Mathematics 11 (2011) 211–239.

[38] J. Guckenheimer, G. Oster, A. Ipaktchi, The dynamics of density dependent population models, J. Math. Biol. 4 (1977) 101–147.

[39] D.G. Aronson, M.A. Chory, G.R. Hall, R.P. McGehee, Bifurcations from an invariant circle for two-parameter families of maps of the plane: a computer-assisted study, Comm. Math. Phys. 83 (1982) 303–354.

[40] R.F. Costantino, R.A. Desharnais, J.M. Cushing, B. Dennis, Chaotic dynamics in an insect population, Science 275 (1997) 389–391.

[41] L.W. Botsford, Dynamics of populations with density-dependent recruitment and age structure, in: S. Tuljapurkar, H. Caswell (Eds.), Structured-Population Models in Marine, Terrestrial, and Freshwater Systems, Population and Community Biology Series, 18, Chapman & Hall, New York, 1997, pp. 371–408.

[42] J.M. Cushing, B. Dennis, R.A. Desharnais, R.F. Costantino, Moving towards an unstable equilibrium: saddle nodes in population systems, J. Anim. Ecol. 67 (1998) 298–306.

[43] H. Seno, A paradox in discrete single species population dynamics with harvesting/thinning. Math. Biosci. 214 (2008) 63–69.

[44] R.M. May, Periodical cicadas, Nature 277 (1979) 347–349.

[45] J.M. Cushing, Cycle chains and the LPA model, J. Differ. Equations Appl. 9 (2003) 655–670.

[46] R. Kon, Nonexistence of Synchronous Orbits and Class Coexistence in Matrix Population Models, SIAM J. Appl. Math. 66 (2006) 616–626.

[47] E. Liz, Global stability and bifurcations in a delayed discrete population model, Int. J. Qual. Theory Differ. Equ. Appl. 3 (2009) 66–80.

[48] C. Conley, Isolated invariant sets and the Morse index, Amer. Math. Soc., Providence, RI, 1978.

[49] M. Mrozek, Leray functor and cohomological Conley index for discrete dynamical systems, Trans. Am. Math. Soc. 318 (1990) 149–178.

[50] A. Szymczak, The Conley index for discrete semidynamical systems, Topology Appl. 66 (1995) 215–240.

[51] K. Mischaikow, M. Mrozek, P. Pilarczyk, Graph approach to the computation of the homology of continuous maps, Foundations of Computational Mathematics 5 (2005) 199–229.

[52] P. Pilarczyk, K. Stolot, Excision-preserving cubical approach to the algorithmic computation of the discrete Conley index, Topology Appl. 155 (2008) 1149–1162.